

Modeling of Copper Zinc Tin Sulfide Solar Cells with Various Buffers Using SCAPS-1D

Han Zhang, Kah-Yoong Chan, and Zi-Neng Ng*

Recently, researchers have shown a strong interest in research on quaternary semiconductor copper zinc tin sulfide (CZTS) photovoltaic cells. These cells have a high absorption coefficient, a direct bandgap, and excellent electrical properties. However, the toxicity of cadmium (Cd) in the cadmium sulfide (CdS) buffer layer in standard CZTS solar cells, can generate severe environmental contamination that is hazardous to humans. As a result, building a Cd-free CZTS solar cell is critical. Meanwhile, given that the peak power conversion efficiency of CZTS solar cells stands at a modest 11%, this study is dedicated to identifying an optimal approach for replacing the environmentally hazardous CdS layers to enhance overall efficiency. SCAPS-1D is a one-dimensional solar cell simulation program commonly used to examine proposed solar cells without building them. This study highlights the performance of CZTS with various nontoxic buffer layers, as well as the key results obtained through numerical research with SCAPS-1D.

1. Introduction

In recent decades, people have become increasingly interested in solar cells that are based on polycrystal cadmium telluride (CdTe), copper indium selenide (CIS), and $\text{CuIn}_x\text{Ga}_{(1-x)}\text{Se}_2$ (CIGS).^[1,2] Even though the photoelectric conversion efficiency of CIGS thin film solar cells has already reached 23%, indium (In), gallium (Ga), and selenium (Se) elements are rare in the natural world, which restricts its development.^[3] CdTe solar cell is a relatively mature technology. However, the element Cd is toxic and harmful to the environment if it is not handled correctly. As a quaternary sulfur compound, $\text{Cu}_2\text{ZnSnS}_4$ (CZTS) has good photoelectric properties and cheap raw materials. CZTS is also a nontoxic and earth-abundant element composition. Therefore, it becomes the most suitable material to replace CIGS and CdTe to lower costs and improve transfer efficiency.^[4] The high solar absorption coefficient over 10^4 cm^{-1} and direct

bandgap between 1.45 and 1.6 eV make CZTS a new version of next-generation photovoltaic material. The structure of the CZTS composite is shown in Figure 1. The position of each element exists on the lattice coordinate. Cuprum (Cu) atoms are at the corner and center of the crystal lattice, while zinc (Zn) atoms are located at the top, bottom, and other sides. Sulfur (S) atoms are shown in the center closest to Cu.^[5] The level of each atom shown in the lattice is similar to the ratio of each element. The compound has a high melting point of 1,269 k, which is suitable for high-temperature synthesis.^[6,7] There are two types of CZTS with unique structures: stannite and kesterite. The arrangements of Cu and Zn atoms are the only noticeable differences between

the two forms.^[8] CZTS usually presents as kesterite (Figure 2) because of its stability.^[8–10] In early reporting of the structure, the 2a position is fully taken by Cu atoms, while mixing Cu and Zn atoms happens at 2c and 2d. Soon after that, Cu atoms are found to be replaced by Zn atoms at the 2a position. Recently, position 2a has been the same as 2c and 2d, a fully disordered kesterite crystal structure. CZTS compound has a high theoretical photoelectric conversion efficiency, which is 32.4%. Due to the excellent resistance to light failure, few internal defects occur in thin film after extended exposure to intense light.^[11] As a result, CZTS has the potential to be utilized in the manufacturing of thin-film solar cells. The structure of a standard thin-film photovoltaic cell incorporating CZTS is depicted in Figure 3. Soda-lime glass (SLG), an absorbing layer, a back contact layer, and a window layer make up the standard structure.

However, several issues regarding technological and material challenges remain to be addressed. First, solar cells utilizing CZTS composition have demonstrated a peak power conversion efficiency (PCE) of approximately 11.0% for CZTS. These values are notably below the efficiencies achieved by CIGS (23.35%) and CdTe (22.1%) technologies.^[12] Researchers use different methods to improve the performance of CZTS solar cells; for example, Su et al. allow the efficiency of CZTS solar cells to exceed 12% through the postannealing device with Cd alloy,^[12] while Liang et al. fabricate high-quality thin film layer by solution-processed spin coating and thermally processed selenization to reduce carrier recombination.^[13] Even though the efficiency has improved, it is still low. Second, in practical manufacturing, enhancing the operational efficiency of kesterite solar cells hinges on the crucial significance of the selenization annealing process. Yu et al. improved the method by supplying a combination of SnS and

H. Zhang, Z.-N. Ng
School of Electrical Engineering and Artificial Intelligence
Xiamen University Malaysia
Jalan Sunsuria, Bandar Sunsuria, Sepang, Selangor 43900, Malaysia
E-mail: zineng.ng@xmu.edu.my

K.-Y. Chan
Centre for Advanced Devices and Systems
Faculty of Engineering
Multimedia University
Persiaran Multimedia, Cyberjaya, Selangor 63100, Malaysia

 The ORCID identification number(s) for the author(s) of this article can be found under <https://doi.org/10.1002/pssb.202300270>.

DOI: 10.1002/pssb.202300270

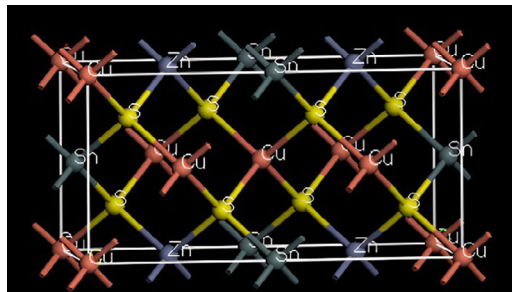


Figure 1. Crystal structure of CZTS. Reproduced with permission.^[5] Copyright 2018, Elsevier.

S during annealing to develop the PCE of solar cells to 12.89%.^[14] Nevertheless, during the annealing process, the high temperature would cause the reaction between the absorber and back contact layer, leading to unfavorable CZTS and a low-quality interface. Thus, the whole performance of the solar cell will be degraded. Zhao introduced an intermediate layer at the back interface to restrain such an effect without considering the annealing supplementary.^[15] A CZTS solar cell with even higher performance will appear if both ways are connected. Furthermore, to minimize the open circuit voltage (V_{oc}) deficit, several studies have focused on substituting elements of CZTS technology, metal ion doping strategy, and postannealing treatment.^[16–19] In addition, the long-term stability and reliability of CZTS solar cells under various operating conditions, including exposure to light, heat, and moisture, are areas of concern. Understanding the degradation mechanisms and finding ways to enhance the stability of CZTS devices is crucial for practical applications.

The conventional configuration of CZTS solar cells calls for the use of CdS as the buffer layer material. However, CdS has a low bandgap, leading to a significant loss of photons. Meanwhile, it is toxic, which would be harmful to the environment. Therefore, a suitable composite with a higher bandgap and nontoxic as a buffer layer is necessary and a current research hotspot. Much research has been done to replace the toxic buffer layer, but so far, work has yet to be done to integrate all statistics about nontoxic buffer layers and make the comparison. This work aims to collect as comprehensive data as possible to illustrate the performance of CZTS solar cells with different

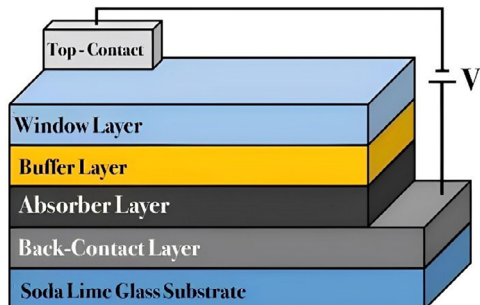


Figure 3. Structure of the traditional CZTS solar cell. Reproduced with permission.^[93] Copyright 2017, Royal Society of Chemistry.

environmentally friendly buffer layers, discuss advantages and drawbacks, and indicate some better solutions.

2. Simulation Software Details

Many studies about CZTS solar cells are based on SCAPS-1D simulation software. The University of Gent invented solar cell capacitance simulator (SCAPS-1D) software. The software can be downloaded from the SCAPS-1D official website for free and is considered the best tool to analyze the proposed solar cell without constructing it. The software employs Newton–Ralphson–Gummel iteration to address the transport and continuity equations, resolving semiconductor and electrostatic behaviors. SCAPS-1D package can simulate a wide range of tunneling and multivalent defect phenomena commonly observed in thin film solar cells. Consequently, it can effectively depict the impact of absorption, energy band alignments, inter and intraband tunneling, defects in energy level, and recombination within thin film solar cells.^[20] It can analyze different families of solar structures, such as CIGS and CuInSe₂, families of crystal solar cells, such as Si and GaAs, and the noncrystal family a-Si. The parameter simulation in practicality in heterojunctions with thin polycrystalline films is very complicated. Because of this, the software employs many electric measurements when it is dark and illuminated at various temperatures.^[21,22] Analysis of the effect of output performance in various parameters of solar cells can also be done, such as the open circuit voltage (V_{oc}), short circuit current density (J_{sc}), fill factor (FF), and the quantum efficiency (QE). Thus,

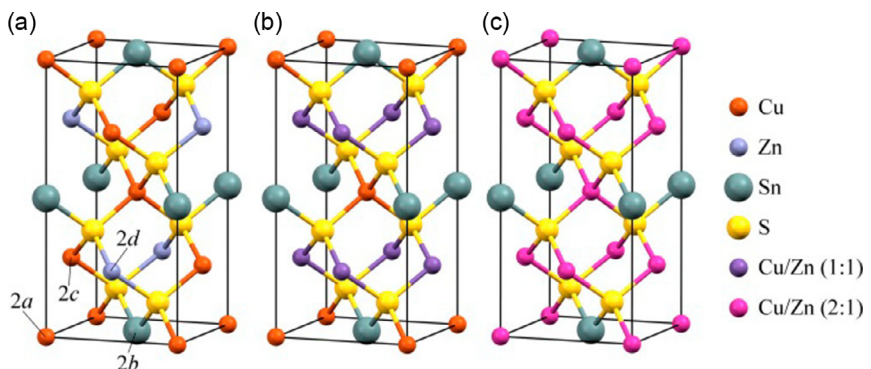


Figure 2. a) Kesterite, b) half-disordered kesterite, and c) fully disordered kesterite crystal structures of CZTS. Reproduced with permission.^[97] Copyright 2017, American Chemical Society.

the following subsections will discuss the accomplishment of CZTS solar cells with various buffer layers using SCAPS-1D.

A simulation study of solar cells offers several advantages compared to experimental approaches and other software tools. For cost efficiency, conducting virtual experiments through simulations significantly reduces costs compared to setting up and running physical experiments. There is no need to purchase materials, equipment, or dedicated lab space. Meanwhile, simulation could save much time. Simulations can run throughout the day, and experiments can be sped up or slowed down as needed. This allows researchers to explore a wide variety of scenarios quickly. However, for physical experiments, depending on the complexity, it can take weeks or even months. In addition, it is more flexible to modify parameters, change conditions, and test different configurations in a virtual environment through simulation. Changes in experimental setups may require significant adjustments, leading to longer lead times and higher costs. Moreover, the use of simulation software is not only secure but also eco-conscious, as it does not entail the use of hazardous materials or generate any waste throughout the entire procedure.

3. Metal Oxide Buffer Layer of CZTS Solar Cell

3.1. Characteristics of Metal Oxide Material

Since solar cells with metal oxide thin films have superior optical transmission, chemical inertness, and terminal stability, they are essential in scientific investigation. $Zn_{1-x}Mg_xO$ is a potential compound to replace the traditional toxic material CdS as a buffer layer.^[23,24] Lee et al. found that the energy gap could be adjusted by modifying the magnesium (Mg) composition, which is a great advantage.^[25] For example, increasing the Mg content from 0 to 0.5 could improve the band gap from 3.2 to 3.9 eV.^[26–28] Maharana et al. used TiO₂, MoO₃, and WO₃ as potential buffer layer choices to develop the CZTS solar cells.^[29] Transition metal oxide materials are suitable for the buffer layer as they can reduce the potential contact restriction.^[30,31] MoO₃ is

superior to other materials for use in solar cells in several respects, including having a low temperature at which it can evaporate, being nontoxic, and having an adequate energy level compatible with most semiconductors. High optical transmission in thin layer WO₃ is advantageous for hole extraction. Additionally, it has a relatively smooth and hydrophobic surface, which aids in forming interface contact with the active layer. Because of its high bandgap (3.0–3.5 eV), it has the potential to dramatically reduce the cost of manufacturing solar cells.^[32] ZnO is also a promising metal oxide buffer layer that has been investigated numerically. It was chosen by Al Zoubi et al. to make further improvements.^[33] Details of the comparison are illustrated in Table 1.

3.2. Improvement in CZTS Solar Cell with Metal Oxide Buffer Layer

The photovoltaic cell that Hedibi et al. created has a ZnMgO buffer layer, and the proposed structure is Mo/CZTS/ZnMgO/i-ZnO/ZnO:Al. ZnO:Al and ZnO are regarded as window layers. The thickness of ZnO:Al varies from 0.02 to 0.325 μm, while ZnO is set from 0.02 to 0.2 μm. As for the buffer layer, the thickness changes from 0.02 to 0.16 μm.^[34] Meanwhile, the CZTS absorber layer's thickness changed from 0.5 to 4 μm. The simulation result on SCAPS-1D shows the best when optimizing the thickness of ZnO:Al, ZnO, and ZnMgO are the same at 0.02 μm and CZTS is 2 μm.^[35] Figure 4 tabulates all results. In Maharana's work, three types of metal oxide buffer layers are investigated they are TiO₂, MoO₃, and WO₃. The three structures are named CTZ, CMZ, and CWZ. The proposed structure is Pt or Ni/CZTS/TiO₂ or MoO₃ or WO₃/ZnO. The CZTS thickness changes from 2 to 3 μm in the CTZ system, varies from 2 to 6 μm in the CMZ system, and sets from 5 to 6 μm in the CWZ system. Meanwhile, each material's buffer layer thickness setting varies: 0.04–0.3 μm for TiO₂, 0.1–1 μm for MoO₃ and 0.01–0.1 μm for WO₃. The window layer remains constant at 10 nm during the simulation. Through the result, to reach the highest efficiency of the PV cell, CZTS thickness is optimized

Table 1. Parameters of metal oxide in SCAPS-1D.

Parameter/Layer	ZnMgO	TiO ₂	MoO ₃	WO ₃	n-ZnO
Thickness [μm]	0.02–0.16	0.04–0.3	0.1–1	0.01–0.1	0.1–2.4
Bandgap [eV]	3.57	3.2	3.8	3.15	3.3–4
Electron affinity [eV]	4.2	4.2	4.1	4.55	4.6
Dielectric permittivity	9	10	9	10	9
CB effective DOS [cm ⁻³]	3×10^8	2×10^{17}	2.2×10^{18}	4.2×10^{18}	2.2×10^{18}
VB effective DOS [cm ⁻³]	1.7×10^{19}	6×10^{17}	1.8×10^{19}	9×10^{18}	1.8×10^{19}
Electron thermal velocity [cm s ⁻¹]	2.4×10^7	1×10^7	1×10^7	1×10^7	1×10^7
Hole thermal velocity [cm s ⁻¹]	1.3×10^7	1×10^7	1×10^7	1×10^7	1×10^7
Electron mobility [cm ² V ⁻¹ s ⁻¹]	3	1×10^2	3×10^1	2×10^1	100
Hole mobility [cm ² V ⁻¹ s ⁻¹]	0.9	2.5×10^2	6	1×10^1	25
Shallow uniform donor density N _D [cm ⁻³]	1×10^{16}	1×10^{17}	1×10^{17}	2×10^{18}	$10^{12}–10^{18}$
Shallow uniform acceptor density N _A [cm ⁻³]	0	0	0	0	0
Defect density N _t [cm ⁻³]	1×10^{14}	1×10^{14}	1×10^{14}	1×10^{14}	1×10^{15}
References	[34,35]	[29]	[29]	[29]	[33]

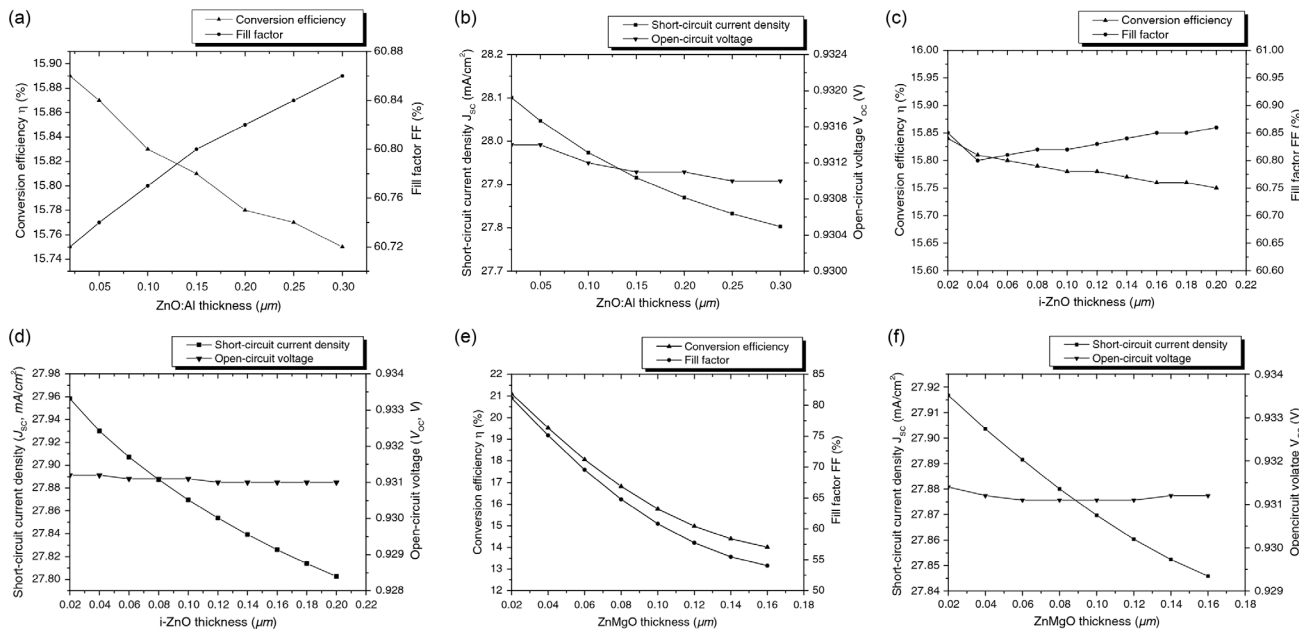


Figure 4. Simulation results of Mo/CZTS/ZnMgO/i-ZnO/ZnO:Al: a) efficiency and FF and b) J_{sc} and V_{oc} versus the thickness of the ZnO:Al layer; c) efficiency and FF and d) J_{sc} and V_{oc} versus the thickness of the i-ZnO layer; e) efficiency and FF and f) J_{sc} and V_{oc} versus the ZnMgO buffer layer thickness. Reproduced with permission.^[35] Copyright 2021, Springer Nature.

to 2.8, 5.2, and 5.1 μm in three systems, respectively. As the acceptor density in CZTS approaches $1 \times 10^{16} \text{ cm}^{-3}$, the efficiency reaches its highest possible value. The CTZ and CMZ systems reach maximum efficiency at $1 \times 10^{16} \text{ cm}^{-3}$ for the donor density in the buffer layer. The CWZ system's maximum efficiency appears when donor density becomes $1 \times 10^{18} \text{ cm}^{-3}$. The optimizing thickness of the buffer layer in the CTZ system is 0.1 μm , in CMZ, it is 0.2 μm , and in the CWZ system is 0.02 μm .^[29,36–38] Mo/MoS₂/CZTS/ZnO/i-ZnO/n-ZnO is proposed by Al Zoubi et al., in which a ZnO buffer layer is used, and their subsequent exploration of the distinctive parameters of the absorber and buffer layer such as thickness, bandgap energy, and carrier concentration. Figure 5 displays all the results. The bandgap energy varies from 1.4 to 1.56 eV, while the thickness of the absorber layer changes from 0.8 to 1.6 μm . At the same time, the acceptor carrier concentration of CZTS is set from 10^{12} to 10^{18} cm^{-3} . After doing simulations, the group concluded that the optimal thickness for the absorber layer is 1.6 μm , the buffer layer is 0.1 μm , 1.4 eV should be energy bandgap, and the suitable carrier concentration is 10^{15} cm^{-3} .^[33]

3.3. Performance of CZTS Solar Cell with Metal Oxide Buffer Layer

All the parameters are set in the software for the structure of CZTS with the ZnMgO buffer layer. Performance results are $\eta = 21.86\%$, $J_{sc} = 27.875 \text{ mA cm}^{-2}$, and $V_{oc} = 0.932 \text{ V}$.^[33] In the work of Maharana et al., the optimizing efficiency of the CTZ system is 20.6% with a CZTS thickness of 2.8 μm and TiO₂ 0.1 μm , the optimizing efficiency of CMT system is 19.3% with CZTS thickness of 5.2 μm and MoO₃ 0.2 μm and the optimizing efficiency of CWZ system is 20.9% with CZTS thickness of 5.1 μm and WO₃

0.03 μm .^[29] The simulation result by Zoubi et al. shows an improvement in J_{sc} and QE parameters, and the maximum efficiency is 19.96%. Compared to a traditional CZTS solar cell with a CdS buffer layer, the current density J_{sc} is around 1.41 mA cm^{-2} higher in the proposed structure, and the photons collection increases.^[35]

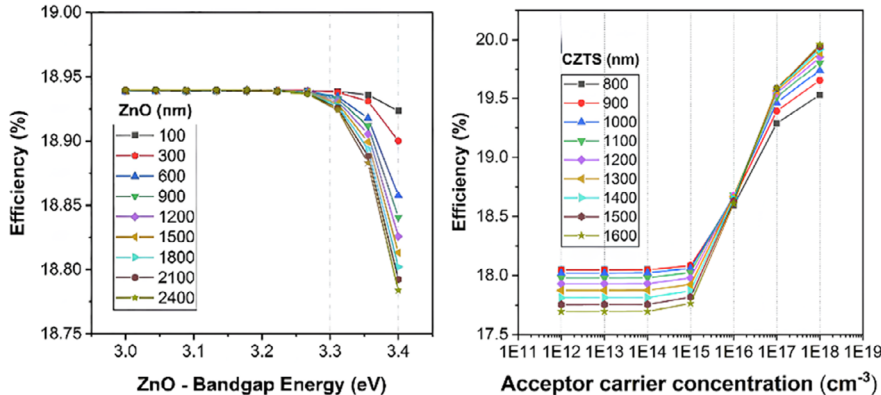
According to Table 2, the proposed structure with $\text{Zn}_{1-x}\text{Mg}_x\text{O}$ metal oxide buffer layer exhibits the best performance with the highest efficiency. That is because ZnMgO is a compound composed of ZnO doped with suitable Mg ions and has a proper lattice, better matched than other metal oxide materials. Moreover, ZnMgO possesses desirable properties such as high radiation resistance, good environmental compatibility, and resistance to chemical corrosion, making it the most promising metal oxide material. Additionally, ZnMgO can achieve the broadest bandgap by adjusting the concentration of Mg ions in the doping process, which can enhance solar cell conversion efficiency by reducing absorption loss. However, in practice, the potential lattice mismatch of ZnMgO can lead to defects and strain within the material, which may affect the overall performance and efficiency of the solar cell.

4. Zinc Sulfide (ZnS) Buffer Layer of CZTS Solar Cell

4.1. Characteristics of ZnS

ZnS is a promising semiconductor that can be applied to CZTS solar cells and is an essential member of the II–VI family.^[39] ZnS is an n-type semiconductor with a bandgap of 3.5–3.8 eV, making it wider than common CdS. Hence, photons with high energy traverse the ZnS buffer layer, arriving at the p-region (CZTS),

(a)



(b)

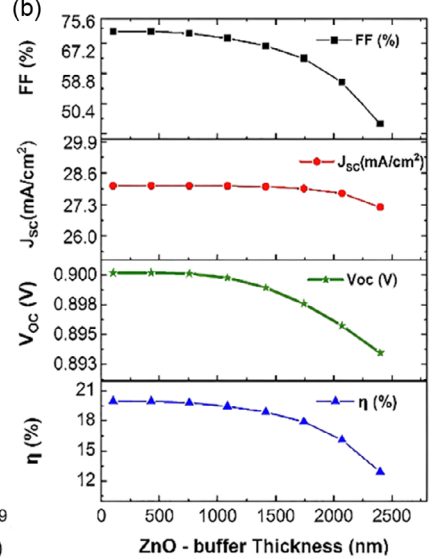


Figure 5. Simulation output results of Mo/MoS₂/CZTS/ZnO/i-ZnO/n-ZnO. Reproduced with permission.^[33] Copyright 2020, Elsevier.

Table 2. Performance of proposed structures.

Reference	Proposed structure	Buffer layer	Absorber layer	Efficiency [%]	V _{OC} [V]	FF [%]	J _{SC} [mA cm^{-2}]
[35]	Mo/CZTS/ZnMgO/i-ZnO/ZnO:Al	ZnMgO (0.02 μm)	CZTS (2 μm)	21.86	0.932	80.10	27.875
[33]	Pt or Ni/CZTS/TiO ₂ /ZnO	TiO ₂ (0.1 μm)	CZTS (2.8 μm)	20.61	0.969	76.73	27.950
[33]	Pt or Ni/CZTS/MoO ₃ /ZnO	MoO ₃ (0.2 μm)	CZTS (5.2 μm)	19.33	0.965	73.40	27.718
[33]	Pt or Ni/CZTS/WO ₃ /ZnO	WO ₃ (0.02 μm)	CZTS (5.1 μm)	20.93	0.969	77.82	27.300
[35]	Mo/MoS ₂ /CZTS/n-ZnO/i-ZnO/n-ZnO	ZnO (0.1 μm)	CZTS (1.6 μm)	19.96	0.898	74.60	27.760

potentially enabling more efficient absorption of shorter solar spectrum wavelengths. For this reason, ZnS could improve the blue response of solar cells by minimizing photon absorption loss.^[40] Furthermore, ZnS demonstrates superior hole mobility, leading to an increased enhancement in the collection efficiency. Both elements, Zn and S, are cheap and abundant in nature. Meanwhile, because of the wide bandgap, ZnS is suitable for doping with many dopants as primary material.^[41] The two crystal structures of ZnS are shown in Figure 6 which are wurtzite (WZ) and zinc blende (ZB) crystal structures.^[42] The cubic of WZ is a low-temperature structure, while the crystal cell of ZB is a high-temperature phase whose melting point could achieve 1,296 k.^[43] The parameters of WZ are $a = b = c = 5.41 \text{ \AA}$, $Z = 4$, and its space group is F4-3m, while the parameters of the ZB lattice are $a = b = 3.82 \text{ \AA}$, $c = 6.26 \text{ \AA}$, $Z = 2$, and the space group is P6₃mc. In addition, the bandgap of ZB is 3.72 eV, while WZ has a higher bandgap of 3.77 eV.^[44] Abd El Halim et al. and Yassine et al. investigated the CZTS solar cell with a ZnS buffer layer through SCAPS-1D; all parameters are illustrated in Table 3.

4.2. Improvement in CZTS Solar Cell with ZnS Buffer Layer

Abd El Halim et al. came up with a structure Mo/CZTS/ZnS/ZnO, while Yassine et al. proposed a similar structure

Mo/CZTS/ZnS/ZnO:F, ZnO:F is ZnO doped with fluorine. The high performance of ZnO:F has been proved, and fluorine (F) is considered a candidate for ZnO.^[45] The composition of the window layer constitutes the primary distinction between the two architectural configurations. Instead of concentrating on the absorber layer's physical properties, Abd El Halim et al. optimized those of the buffer layer. Yassine et al. looked into the thickness of the CZTS layer and the ZnO:F window layer simultaneously. The two analyses evaluate the carrier concentration and buffer layer thickness. The ZnS that the Halim team used has a thickness that ranges from 30 to 100 nm, and the doping concentration ranges from 1×10^{17} to $1 \times 10^{18} \text{ cm}^{-3}$. This is done so that the team can determine the optimal thickness and concentration for ZnS. The result in Figure 7 shows that the thinner the buffer layer, the higher the efficiency is, and the most suitable thickness for ZnS is 30 nm. Then, fix the thickness of the buffer layer and adjust the concentration. Finally, the optimizing doping concentration for ZnS is $5 \times 10^{17} \text{ cm}^{-3}$.^[46] For Yassine's study, CZTS thickness varies from 3.2 to 4.1 μm . As a result, the conversion efficiency reaches the maximum and remains constant after 3.9 μm . Therefore, the optimizing thickness is set to 3.9 μm . After that, the doping concentration of the CZTS absorber layer changes from 1×10^{15} to $8 \times 10^{16} \text{ cm}^{-3}$. The result shows that the efficiency approaches peak value when the concentration is $9 \times 10^{15} \text{ cm}^{-3}$.^[47]

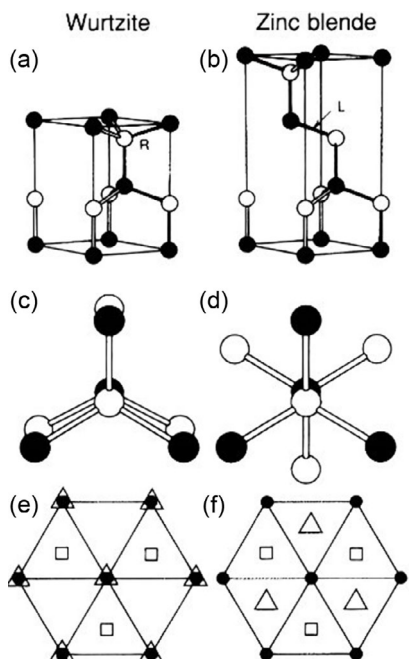


Figure 6. a) Wurtzite structure and b) zinc blende structure; headedness of fourth interatomic bond for c) WZ and d) ZB; conformation of staggered and eclipsed dihedral for e) WZ and f) ZB. Reproduced with permission.^[43] Copyright 1992, American Chemical Society.

Table 3. Parameters of ZnS in SCAPS-1D.

Parameter/Layer	ZnS	ZnS
Thickness [μm]	0.05	0.05
Bandgap [eV]	3.3	3.7
Electron affinity [eV]	4.4	4.5
Dielectric permittivity	10	9
CB effective DOS [cm ⁻³]	2.2×10^{18}	2.2×10^{18}
VB effective DOS [cm ⁻³]	1.8×10^{19}	1.8×10^{19}
Electron thermal velocity [cm s ⁻¹]	1×10^7	1×10^7
Hole thermal velocity [cm s ⁻¹]	1×10^7	1×10^7
Electron mobility [cm ² V ⁻¹ s ⁻¹]	100	100
Hole mobility [cm ² V ⁻¹ s ⁻¹]	25	25
Shallow uniform donor density N _D [cm ⁻³]	1×10^{18}	1×10^{17}
Shallow uniform acceptor density N _A [cm ⁻³]	0	0
Defect density N _t [cm ⁻³]	1×10^{14}	1×10^{14}
References	[46]	[47]

4.3. Performance of CZTS Solar Cell with ZnS Buffer Layer

After setting optimizing values for the Mo/CZTS/ZnS/ZnO structure, the performance parameters successfully improved. The efficiency of the solar cell is 12.78%, $J_{SC} = 25.257 \text{ mA cm}^{-2}$, FF = 65.311%, and $V_{OC} = 0.777 \text{ V}$.^[46] As a consequence of this, the performance of the ZnS demonstrates an improvement, demonstrating the dependability of

ZnS material as a replacement for CdS. Nevertheless, FF is low, severely impacting solar cell stability. Significant traps for charge carriers are formed within a heavily doped buffer layer, thereby raising the likelihood of interactions. Additionally, the charge carrier lifetime demonstrates an inverse relationship with trap concentration. Therefore, the recombination rate increases, leading to a decrease in FF. For the second structure, the window layer changes from 0 to 200 nm in simulation, and V_{OC} keeps constant with the increase of ZnO:F while FF, J_{SC} , and efficiency decrease. The final performance parameters are efficiency = 14.61%, FF = 71.94%, $J_{SC} = 25.40 \text{ mA cm}^{-2}$, and $V_{OC} = 0.79 \text{ V}$.^[47] The result, illustrated in Table 4, shows that the structure with ZnO:F window layer has higher efficiency. F could increase the free electron concentration and film conductivity.^[48,49] However, even though solar cell doped with F performs better, it harms the environment, which is not suggested for large-scale applications.

Among two similar proposed structures in Table 4, the one with the ZnO:F window layer performs better, primarily in the FF and efficiency area. Though using ZnO:F is not recommended, it gives a new idea for further study to improve the solar cell. Doping some nontoxic atoms or ions such as boron, aluminum (Al), and In to develop conductivity of the window layer and increase the stability of electrical properties is a way to enhance the characteristics of CZTS solar cells. ZnS is not a good choice as a buffer layer, as it has a low FF, which can shorten the solar cell's lifetime, and its PCE is lower than other materials. However, it does provide an alternative to replace the toxic material CdS.

5. Indium (III) Sulfide (In_2S_3) Buffer Layer of CZTS Solar Cell

5.1. Characteristics of In_2S_3

As a potential successor to the CdS buffer layer, In_2S_3 is an intriguing contender since In_2S_3 is environmentally friendly and has optimal conductivity and a suitable bandgap from 2.1 to 2.9 eV.^[50–52] It belongs to the binary semiconductor, a member of the III–VI compound family. There are three phases of In_2S_3 , α , β , and γ . β - In_2S_3 is most commonly used as it is suitable for room temperature, while the other two phases are commonly used at a higher temperature. α - In_2S_3 is a cubic structure, while β - In_2S_3 is a spinel-type structure with a tetragonal phase. In addition, γ - In_2S_3 is a trigonal phase.^[53] The structure of the β - In_2S_3 unit cell is shown in Figure 8; gray balls present element In, while tetrahedral bonds are thicker for better identification.^[54] Vacancies lie on a 4_1 -screw axis parallel to the crystal's c -axis. Meanwhile, the sides of the unit cell are presented by a black line. Only a thin film buffer layer, In_2S_3 , which allows light to pass through, is needed to improve the solar cells as the compound can absorb short-spectrum wavelengths.^[55] However, more numerical simulation is needed due to the limited understanding of CZTS/ In_2S_3 heterojunction solar cells. Recently, more and more studies focusing on In_2S_3 are coming out. Parameters of the In_2S_3 buffer layer in SCAPS-1D of three teams are illustrated in Table 5.

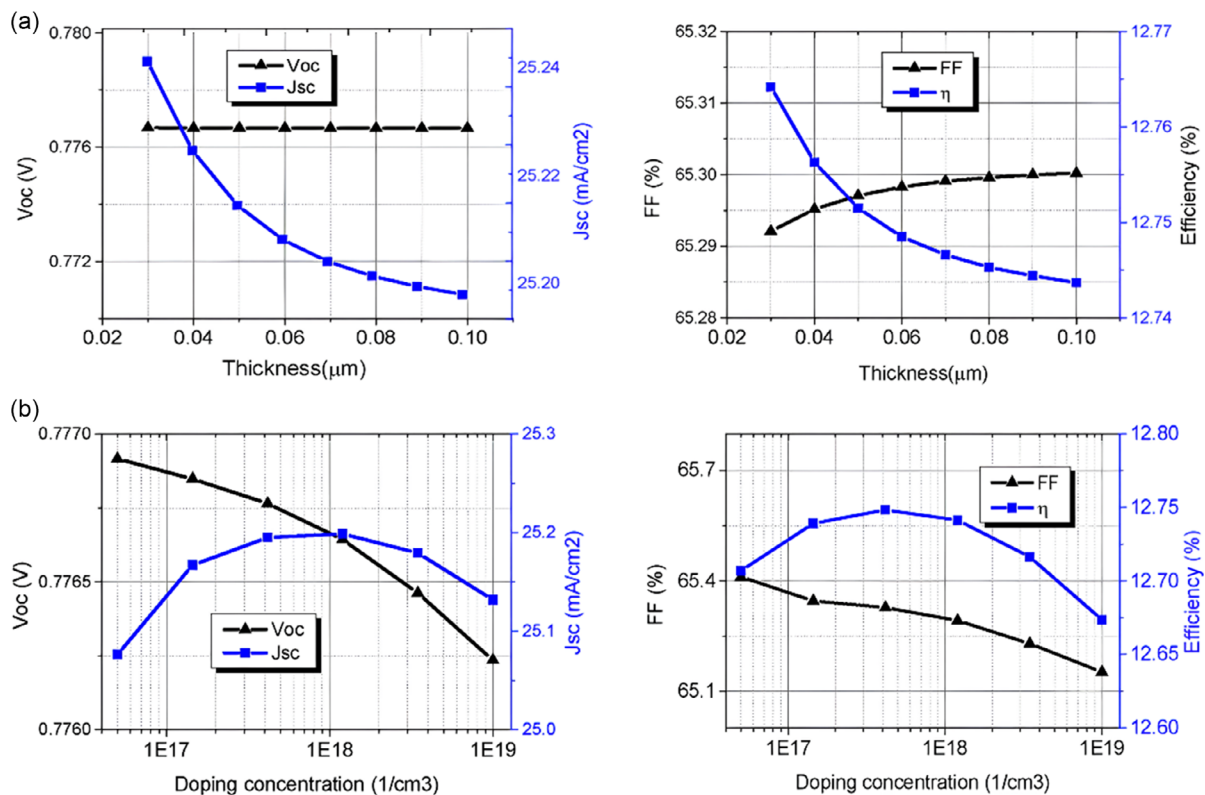


Figure 7. Simulation output results of Mo/CZTS/ZnS/ZnO: Performance versus a) thickness and b) doping concentration of buffer layer. Reproduced with permission.^[46] Copyright 2020, Elsevier.

Table 4. Performance of proposed structures.

Reference	Proposed structure	Buffer layer	Absorber layer	Efficiency [%]	V _{oc} [V]	FF [%]	J _{sc} [mA cm^{-2}]
[46]	Mo/CZTS/ZnS/ZnO	ZnS (0.03 μm)	CZTS (2.5 μm)	12.78	0.777	65.31	25.257
[47]	Mo/CZTS/ZnS/ZnO:F	ZnS (0.002 μm)	CZTS (3.9 μm)	14.61	0.790	71.94	25.400

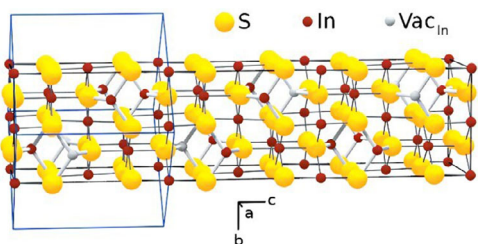


Figure 8. A unit cell of β -In₂S₃. Reproduced with permission.^[54] Copyright 2004, Elsevier.

5.2. Improvement in CZTS Solar Cell with In₂S₃ Buffer Layer

Lin et al. improved the efficiency of CZTS/In₂S₃ in 2014 with the proposed structure Mo/CZTS/In₂S₃/ZnO/ZnO:Al of solar cells. In this structure, n-ZnO performs as a connection layer, while ZnO:Al is regarded as a window layer. Through trial and error, optimizing parameters are obtained. The thickness of CZTS is 3,000 nm, the carrier density is $1 \times 10^{17} \text{ cm}^{-3}$, the defect density

Table 5. Parameters of In₂S₃ in SCAPS-1D.

Parameter/Layer	In ₂ S ₃	In ₂ S ₃	In ₂ S ₃
Thickness [μm]	0.05	0.05	0.05
Bandgap [eV]	2.8	2.8	2.1
Electron affinity (eV)	4.7	4.7	4.2
Dielectric permittivity	13.5	13.5	13.5
CB effective DOS [cm^{-3}]	1.8×10^{19}	1.8×10^{19}	1.8×10^{19}
VB effective DOS [cm^{-3}]	4×10^{13}	4×10^{13}	4×10^{13}
Electron thermal velocity [cm s^{-1}]	1×10^7	1×10^7	1×10^7
Hole thermal velocity [cm s^{-1}]	1×10^7	1×10^7	1×10^7
Electron mobility [$\text{cm}^2 \text{V}^{-1} \text{s}^{-1}$]	400	400	400
Hole mobility [$\text{cm}^2 \text{V}^{-1} \text{s}^{-1}$]	210	210	210
Shallow uniform donor density N_D [cm^{-3}]	1×10^{17}	1×10^{17}	9.8×10^{18}
Shallow uniform acceptor density N_A [cm^{-3}]	10	10	0
Defect density N_t [cm^{-3}]	1×10^{14}	1×10^{18}	1×10^{14}
References	[56]	[52]	[58]

is $1 \times 10^{12} \text{ cm}^{-3}$, the thickness of In_2S_3 is 20 nm, and the carrier density is $1 \times 10^{17} \text{ cm}^{-3}$.^[52] Tripathi et al. 2021 developed a new structure Mo/MoS₂/CZTS/ In_2S_3 /i-ZnO/n-ITO. MoS₂ here is the interface layer, which has a thickness of 100 nm, while the indium tin oxide ITO is a 60 nm transparent conducting oxide film. The optimizing thickness of CZTS and In_2S_3 are 2 μm and 40 nm, respectively. Meanwhile, the picked optimizing donor concentration is $3 \times 10^{17} \text{ cm}^{-3}$.^[56]

In traditional p-n-junction solar cells, the recombination speed of minority carriers at the back surface is significantly elevated due to ohmic contact. This stems from an analysis of the minority-carrier continuity equation in the base region. If the minority-carrier diffusion length is on par with or surpasses the base width, it is clear that the recombination at the back surface plays a critical role in constraining both the short-circuit current density and the open-circuit voltage of the cell. Incorporating a low-high (L-H) junction in proximity to the rear surface of the solar cell can yield an efficient reduction in the surface recombination velocity.^[57] Therefore, adding a back surface field (BSF) could be a new way to improve solar cells. Rachidy et al. added a CZTSe layer to form a BSF layer to increase the efficiency for ZnO:Al/ In_2S_3 /CZTS/CZTSe/Pt. BSF pushes the minority carrier to the front contact layer rather than the back layer by generating a drift. It consists of a high doping area behind the solar cell surface. A p-n junction is formed between high doped and low-doped interface, and an electric field is generated on the interface, which prevents the minority carrier from flowing in the back surface. Hence, the minority carrier density remains elevated within the device's interior. The cell performance could be developed. The reason behind this is the potential barrier created by the p+p junction, preventing the recombination of minority carriers at the back surface of the cell. Additionally, the spike between CZTS and CZTSe (Figure 9) facilitates the pathway for photogenerated holes to reach the back contact, making it more favorable. The impact of BSF thickness is investigated. The value varies from 0.04 to 0.2 μm . Figure 10 depicts that PCE increases from 28.99% to 29.80% with the increasing thickness of the BSF layer. A slight drop occurs in FF since the short lifespan of the minority carriers arises from the elevated carrier concentration at the cell's rear end. To balance the result, 0.1 μm is chosen to be the suitable value. In addition, the optimum absorber layer CZTS is 2 μm while the optimizing

thickness of In_2S_3 is 0.05 μm . The acceptor concentration in the CZTS layer is set at 10^{16} cm^{-3} .^[58]

5.3. Performance of CZTS Solar Cell with In_2S_3 Buffer Layer

Results from the simulation are illustrated in Table 6. The simulation conditions are the same for all the teams; the temperature is set to 300 K, and the standard for lighting is AM.1.5. The efficiency of CZTS with In_2S_3 buffer layer has been improved to 19.28% through Lin's study. Other performance parameters are $J_{\text{SC}} = 23.37 \text{ mA cm}^{-2}$, $V_{\text{OC}} = 0.958 \text{ V}$, and $\text{FF} = 86.13\%$.^[52] The new structure proposed by Tripathi et al. gets an efficiency of 19.03%, $V_{\text{OC}} = 0.795 \text{ V}$, $J_{\text{SC}} = 30.060 \text{ mA cm}^{-2}$, and $\text{FF} = 79.63\%$.^[56] After inserting the BSF layer CZTSe, Rachidy et al. successfully increased the efficiency to 32.50% while other parameters are $V_{\text{OC}} = 0.993 \text{ V}$, $J_{\text{SC}} = 50.690 \text{ mA cm}^{-2}$, and $\text{FF} = 64.60\%$.^[58] Among the three simulation results, inserting a CZTSe layer could dramatically enhance the performance of the photovoltaic cell. Although the window layer was different between studies, it was shown to have minimal impact on the performance of the solar cell. BSF has a considerable responsibility for increasing the PCE of the solar cell. In the study of Rachidy, rather than a p/n junction like a standard solar cell, it uses an n/p/p+ junction. The p/p+ junction establishes an inherent electric field aligned with the p/n junction, amplifying the short-circuit current, while the shared applied voltage between the two junctions reduces the dark current.^[59] Meanwhile, through investigation, a thinner buffer and absorber layer would cause higher efficiency photovoltaic cells. In_2S_3 buffer layer with suitable parameters improves CZTS solar cells' performance and prevents environmental pollution. However, the chemical element In is scarce; therefore, more investigations on buffer layer material are needed.

The most recommended proposed structure with an In_2S_3 buffer layer is the one with a BSF layer, which gains the highest efficiency and J_{SC} . Besides the BSF layer helps form the p-n junction to push the minority carrier into the front contact, doping window layer ZnO with Al ions also increases the conductivity of the CZTS solar cell. In addition, the back contact layer Pt has higher metal work than Mo, which plays a role in developing efficiency. Even though the FF is the lowest since forming the p-n junction, adding a BSF layer provides a creative method to improve CZTS solar cells.

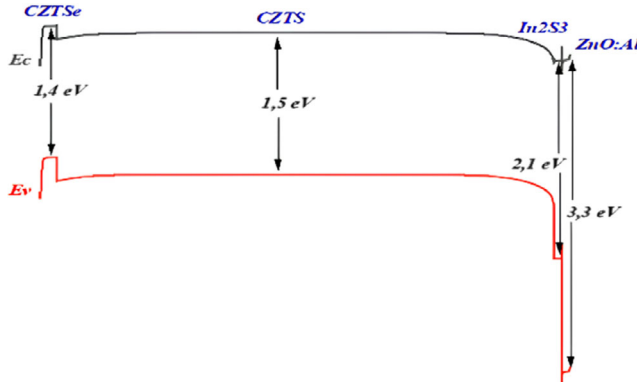


Figure 9. Energy bandgap of ZnO:Al/ In_2S_3 /CZTS/CZTSe/Pt. Reproduced with permission.^[58] Copyright 2022, Elsevier.

6. Molybdenum Disulfide (MoS₂) Buffer Layer of CZTS Solar Cell

6.1. Characteristics of MoS₂

The buffer layer plays a role in forming the p-n junction. Meanwhile, the buffer layer should have a large bandgap to reduce the absorption loss, ensure minimum recombination, and maximize the optical transmission. Therefore, MoS₂ is now a potential material for the buffer layer.^[60,61] This material is unreactive and insensitive to oxygen and some particular acids. It also has a suitable bandgap of 1.23 eV and a high absorption coefficient of more than 10^{14} cm^{-1} .^[62,63] MoS₂ is a semiconductor that provides a suitable energy bandgap for PV

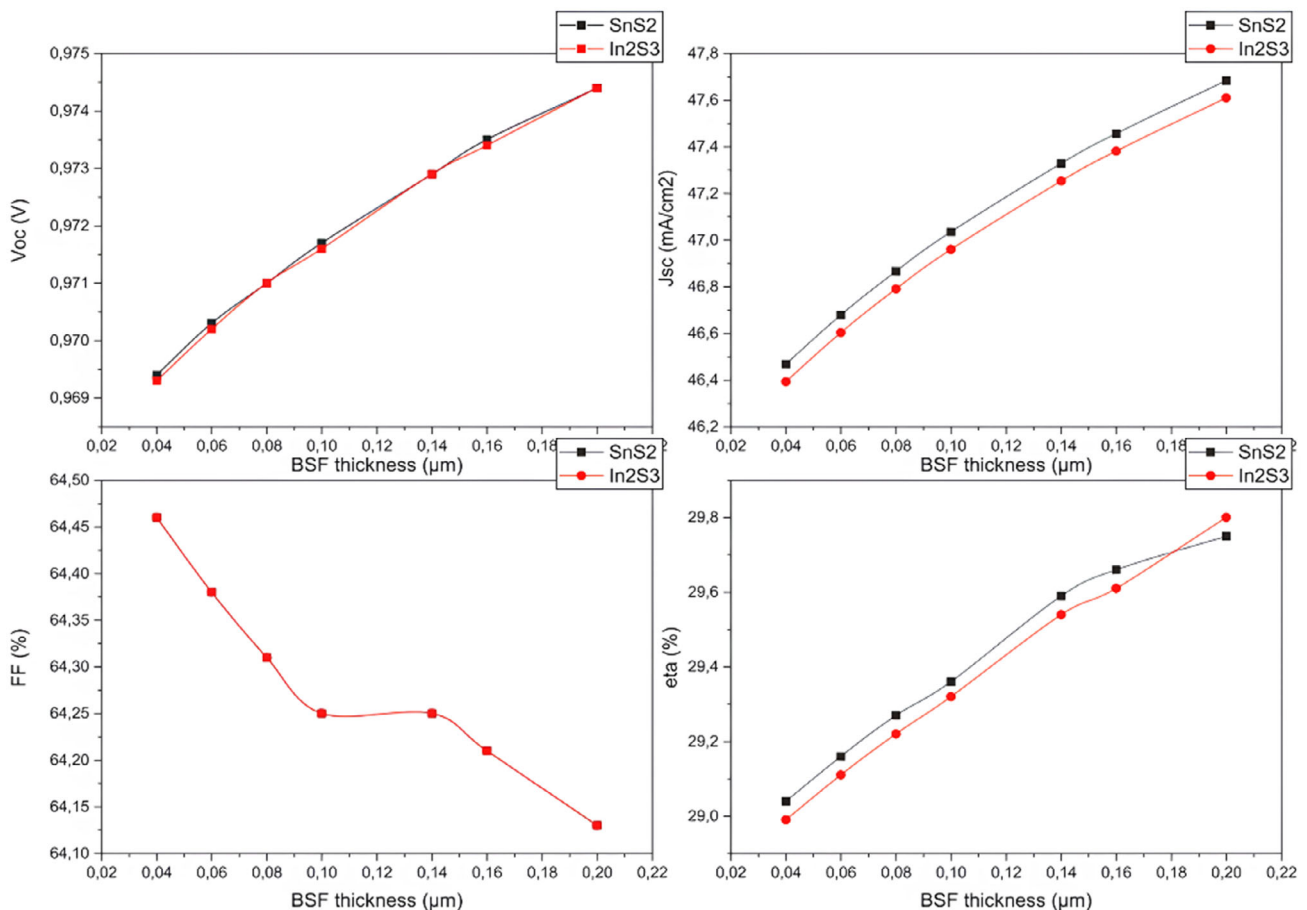


Figure 10. Performance of solar cell for the thickness variation of BSF layer. Reproduced with permission.^[58] Copyright 2022, Elsevier.

Table 6. Performance of proposed structures.

Reference	Proposed structure	Buffer layer	Absorber layer/BSF	Efficiency [%]	V _{oc} [V]	FF [%]	J _{sc} [mA cm ⁻²]
[52]	Mo/CZTS/In ₂ S ₃ /ZnO/ZnO:Al	In ₂ S ₃ (0.02 μm)	CZTS (2.5 μm)	19.28	0.958	86.31	23.37
[56]	Mo/MoS ₂ /CZTS/In ₂ S ₃ /i-ZnO/n-ITO	In ₂ S ₃ (0.04 μm)	CZTS (3 μm)	19.03	0.795	79.63	30.06
[58]	Pt/CZTSe/CZTS/In ₂ S ₃ /ZnO:Al/FTO	In ₂ S ₃ (0.05 μm)	CZTS (2 μm)	32.50	0.993	64.60	50.69

applications.^[64,65] The bandgap of 1.23 eV is ideal for capturing photons with lower energy levels, particularly in the near-infrared range. This extends the range of the solar spectrum that the solar cell can effectively convert into electricity. In comparison, materials with higher band gaps may miss out on these lower-energy photons, limiting the overall efficiency of the cell, especially in low-light conditions. Meanwhile, the bandgap study of Ferdaous et al. shows that MoS₂ with a low band gap is beneficial to CZTS thin film solar cells.^[66] Three phases of MoS₂ have been reported, which are trigonal, hexagonal, and rhombohedral structures, shown in **Figure 11** and corresponding to T, H, and R.^[67] Each belongs to a different point group; the trigonal phase is in D_{6d}, the hexagonal structure is in D_{6h}, and the rhombohedral phase belongs to C_{3v}.^[68] As 2H is a thermodynamically stable phase, it usually exists in natural MoS₂ crystals such as molybdenite. The other two phases are shown during synthetic MoS₂

and are metastable. Mo-S coordinate in 1T is octahedral, while the coordinate is trigonal prismatic in 2H and 3R phases.^[69] Two teams used SCAPS-1D to investigate the CZTS solar cell with MoS₂ buffer layer. The parameters are shown in **Table 7**.

6.2. Improvement in CZTS Solar Cell with MoS₂ Buffer Layer

Bouarissa et al. proposed a structure of CZTS solar cells Mo/CZTS/MoS₂/ZnO. At the same time, Ghosh et al. used graphene (GnP) as a transparent conducting layer to construct the structure Mo/CZTS/MoS₂/ZnO/GnP. During simulation in the first structure, the thickness of ZnO varies from 0.01 to 0.24 μm. When the thickness of the window layer increases, J_{sc} decreases nonlinearly while V_{oc} remains almost constant. The efficiency trend behaves like J_{sc}. Therefore, the best thickness is 0.1 μm for ZnO. For the buffer layer, the thickness of MoS₂ is set from 0.01

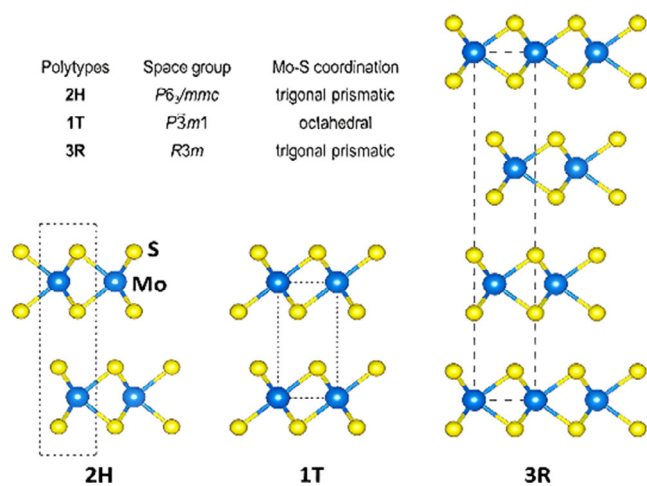


Figure 11. Crystal structures of bulk MoS_2 . Reproduced with permission.^[67] Copyright 2018, Wiley-VCH.

Table 7. Parameters of MoS_2 in SCAPS-1D.

Parameter/Layer	MoS_2	MoS_2
Thickness [μm]	0.01–0.2	0.02–0.18
Bandgap [eV]	1.23	1.3
Electron affinity [eV]	4.2	4
Dielectric permittivity	4	4
CB effective DOS [cm^{-3}]	7.5×10^{17}	7.5×10^{17}
VB effective DOS [cm^{-3}]	1.8×10^{18}	1.8×10^{18}
Electron thermal velocity [cm s^{-1}]	1×10^5	1×10^5
Hole thermal velocity [cm s^{-1}]	1×10^7	1×10^7
Electron mobility [$\text{cm}^2 \text{ V}^{-1} \text{ s}^{-1}$]	100	100
Hole mobility [$\text{cm}^2 \text{ V}^{-1} \text{ s}^{-1}$]	150	150
Shallow uniform donor density N_D [cm^{-3}]	1×10^{18}	1×10^{21}
Shallow uniform acceptor density N_A [cm^{-3}]	0	0
Defect density N_t [cm^{-3}]	1×10^{13}	1×10^{13}
References	[69,70]	[99]

to $0.2 \mu\text{m}$. With the increase of MoS_2 , the parameter increases while the efficiency has the same trend and reaches the highest value when the thickness of MoS_2 is $0.2 \mu\text{m}$. Thus, the best thickness of the buffer layer is $0.2 \mu\text{m}$. The same research steps are used in deciding the thickness of CZTS, and the suitable thickness is $0.1 \mu\text{m}$.^[70] All results are displayed in **Figure 12**. In the second structure, as the graphene owns high conductivity, transparency, and appropriate optical and electrical characteristics, it is preferred as the window layer.^[71] Meanwhile, compared to other traditional conducting oxide layers, it has better thermal stability. Graphene is more widely used than indium tin oxide (ITO) since the cost of producing ITO is expensive and element In is rarer.^[72] To guarantee greater transparency, the optimizing window layer is set to $0.002 \mu\text{m}$.^[73] The thickness of MoS_2 in software varied from 0.02 to $0.18 \mu\text{m}$. As the performance parameters do not increase significantly after $0.04 \mu\text{m}$, the thickness of

MoS_2 is set to be $0.04 \mu\text{m}$. The thickness of CZTS is set from 0.5 to $4 \mu\text{m}$; according to the observation, the efficiency of design increases exponentially until the thickness of CZTS reaches up to $0.2 \mu\text{m}$. Therefore, the optimizing thickness of the absorber layer is $0.2 \mu\text{m}$. For investigating the effect of doping density on the CZTS layer, the absorber layer's concentration value varies from 1×10^{11} to $1 \times 10^{18} \text{ cm}^{-3}$. Through the result, other performance parameters all increase with the increasing doping concentration, except for short-circuit current density. After the doping, concentration on the CZTS layer reaches $1 \times 10^{16} \text{ cm}^{-3}$, all the solar parameters increase slightly. Thus, the optimizing doping density of the absorber layer is $1 \times 10^{16} \text{ cm}^{-3}$.

6.3. Performance of CZTS Solar Cell with MoS_2 Buffer Layer

The performance of ZnO/MoS_2 and GnP/MoS_2 cells is shown in **Table 8**. The best thickness of the suggested solar cell by Bouarissa et al. is $0.1 \mu\text{m}$ for the window layer, $0.2 \mu\text{m}$ for the buffer layer, and $1 \mu\text{m}$ for the absorber layer. Furthermore, the solar cell's characteristic parameters are $\eta = 23.69\%$, $J_{\text{SC}} = 28.96 \text{ mA cm}^{-2}$, $V_{\text{OC}} = 0.84 \text{ V}$, and $\text{FF} = 85\%.$ ^[70] In the study of Ghosh, the compound material GnP/MoS_2 overcomes its drawbacks due to its beneficial physical and chemical properties. The composite constitutes heterostructures in specific ways. Graphene and MoS_2 possess integral physical features and parallel lattice patterns, optimizing solar cell performance.^[74] After optimizing, the whole performance of the solar cell is improved, with the 40 nm thickness of buffer layer, $2 \mu\text{m}$ thickness of absorber layer, and $1 \times 10^{16} \text{ cm}^{-3}$ doping density, the J_{SC} achieves 25.3 cm^{-3} , $V_{\text{OC}} = 0.852 \text{ V}$, $\text{FF} = 84.67\%$, and the efficiency becomes $18.27\%.$ ^[71] This study helps pave the way for the eventual production of CZTS solar cells, which are harmless to humans and the environment. While MoS_2 has some favorable properties, such as its stability and electronic structure, it also presents certain disadvantages. For MoS_2 manufacturing, the worse-matched band offsets with CZTS can lead to significant energy losses, reducing the solar cell's overall efficiency.

Although using GnP material as a window layer is feasible, ZnO is more appropriate due to its high transmittance of up to 90% in the visible light range and its lattice compatibility with MoS_2 . Hence, GnP is not a promising alternative to ZnO as a window layer, but it represents an innovative approach to constructing a CZTS solar cell.

7. Zinc Selenide (ZnSe) Buffer Layer of CZTS Solar Cell

7.1. Characteristics of ZnSe

ZnSe is an attractive option for use in CZTS solar cells as a replacement for the hazardous buffer layer CdS since it has a direct bandgap of 2.7 eV .^[75] This makes ZnSe an excellent choice for use in CZTS sun cells. There are two different allotropes: hexagonal wurtzite (W) and cubic zinc-blende (ZB), available for ZnSe. As a binary octet semiconductor, its structures are shown in **Figure 13**. The main distinction between ZB and W is the dihedral configuration or relative headedness of the fourth

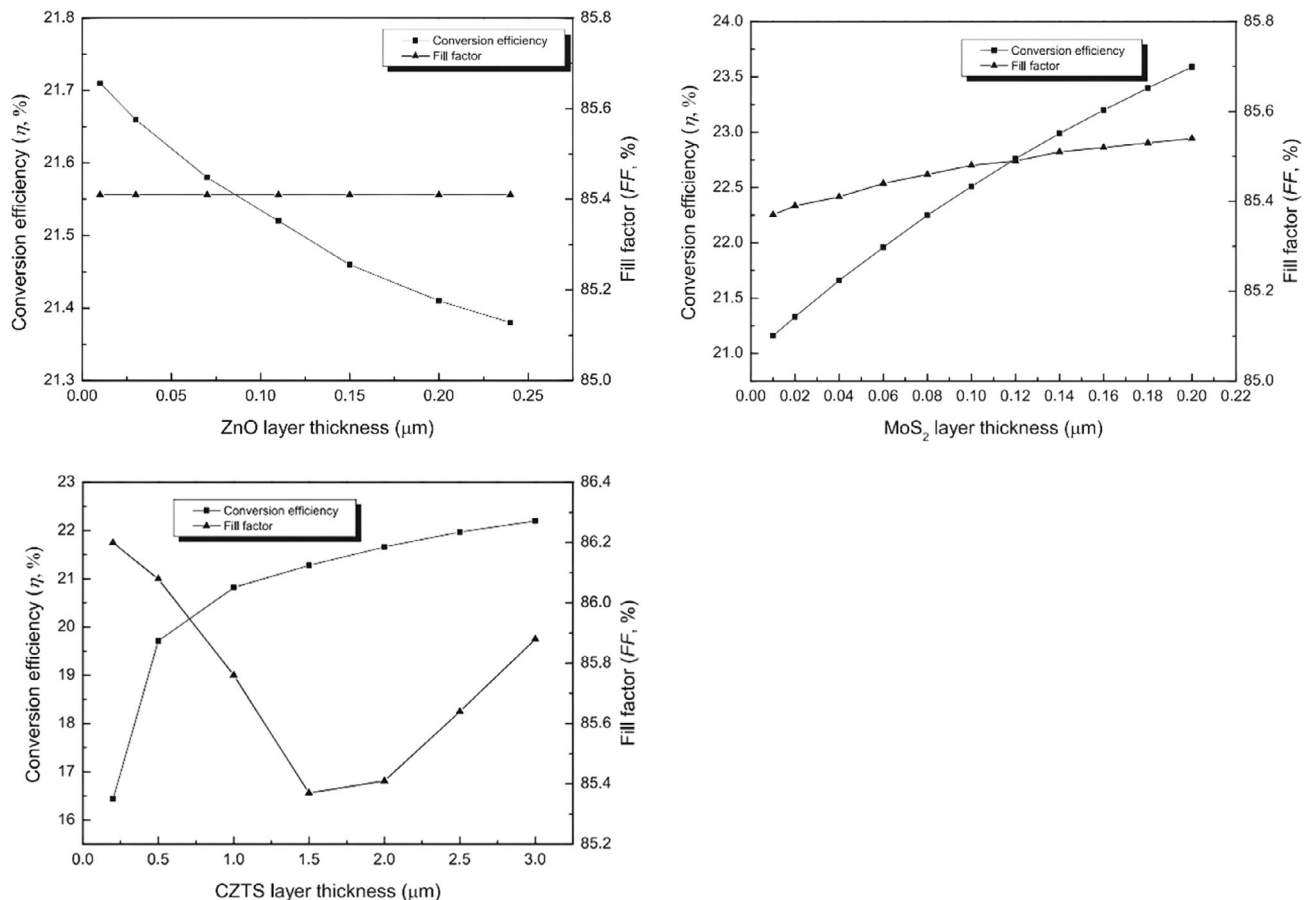


Figure 12. Simulation output result of Mo/CZTS/MoS₂/ZnO. Reproduced with permission.^[70] Copyright 2020, Elsevier.

Table 8. Performance of proposed structures.

Reference	Proposed structure	Buffer layer	Absorber layer	Efficiency [%]	V _{oc} [V]	FF [%]	J _{sc} [mA cm ⁻²]
[70]	Mo/CZTS/MoS ₂ /ZnO	MoS ₂ (0.2 μm)	CZTS (0.1 μm)	23.69	0.840	85.00	28.96
[71]	Ni/CZTS/MoS ₂ /GnP	MoS ₂ (0.04 μm)	CZTS (2.0 μm)	18.27	0.852	84.76	25.30

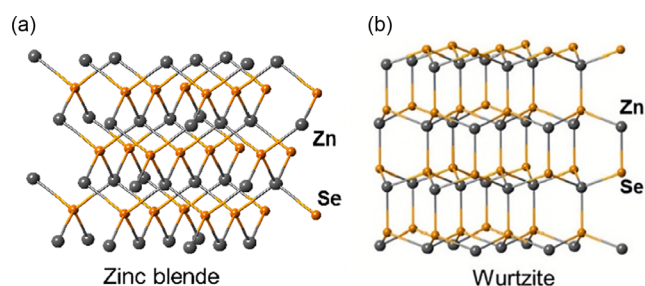


Figure 13. Two different allotropes a) ZB and b) W of ZnSe. Reproduced with permission.^[76] Copyright 2016, Elsevier.

interatomic bond. In the structure of W, the ligand of a tetrahedron is composed by zinc (Zn) atoms and selenium (Se) atoms through the ABABAB pattern. In contrast, the structure of the ZB unit cell is stacked in an ABCABC pattern. The parameters of ZB

lattice are $a = b = c = 5.68 \text{ \AA}$, and ZB lattice belongs to space group F4-3m. W structure is in space group = P63mc, and its parameters are $a = b = 3.98 \text{ \AA}$ and $c = 6.53 \text{ \AA}$.^[76] Even though the ZB structure is in the low-temperature ground state, ZnSe shows the polytypism of so-called W-ZB as the total energy difference is relatively low between the two structures.^[43] Teams of Srivastava, Tousif, and Talukder are investigating CZTS solar cells with a ZnSe buffer layer, and all parameters for simulation are shown in Table 9.

7.2. Improvement in CZTS Solar Cell with ZnSe Buffer Layer

Two different structures, Mo/CZTS/ZnSe/ZnO/ZnO:Al and Mo/CZTS/CZTSe/ZnSe/ZnO/ZnO:Al, are proposed by Srivastava et al. Optimizing the absorber layer's doping concentration, thickness, and fault density improves the solar cell's overall performance. CZTS is varied in a thickness range from 0.5 to

Table 9. Parameters of ZnSe in SCAPS-1D.

Parameter/Layer	ZnSe	ZnSe
Thickness [μm]	0.06	0.03–0.07
Bandgap [eV]	2.9	2.7
Electron affinity [eV]	4.09	4.2
Dielectric permittivity	10	8.1
CB effective DOS [cm^{-3}]	1.5×10^{18}	2.2×10^{18}
VB effective DOS [cm^{-3}]	1.8×10^{18}	1.8×10^{19}
Electron thermal velocity [cm s^{-1}]	1×10^7	1×10^7
Hole thermal velocity [cm s^{-1}]	1×10^7	1×10^7
Electron mobility [$\text{cm}^2 \text{V}^{-1} \text{s}^{-1}$]	50	100
Hole mobility [$\text{cm}^2 \text{V}^{-1} \text{s}^{-1}$]	20	25
Shallow uniform donor density N_D [cm^{-3}]	5.5×10^{18}	2×10^{18}
Shallow uniform acceptor density N_A [cm^{-3}]	0	0
Defect density N_t [cm^{-3}]	1×10^{14}	5.5×10^{14}
References	[77]	[80]

3.5 μm . The optimal CZTS thickness, determined by simulation, is 1.5 μm . Since the naturally occurring CuZn antisite and Cu vacancy, CZTS and CZTSe are natively p-type semiconductors. It is impossible to avoid both faults due to the limited forming energy. Therefore, there is no n-type doping. During simulation, the concentration of the CZTS doping agent varied from 10^{13} to

10^{19} cm^{-3} . According to the findings, both the efficiency and fill factor of CZTS have reached their peaks. The defect density of the absorber layer is set from 10^{11} to 10^{18} cm^{-3} . It is noticed that the efficiency declines steeply after the defect concentration of 10^{15} cm^{-3} . Thus, the optimizing doping concentration is chosen to be 10^{11} cm^{-3} . Meanwhile, the interface defect density is set to $5 \times 10^{11} \text{ cm}^{-3}$. Current leakage will occur if the buffer layer is of insufficient thickness; hence, this should be avoided. Through simulation, the optimal thickness of ZnSe is determined to be 60 nm. The thickness of the two materials is different for the combined absorber layer CZTS and CZTSe. The improved width values are 1 μm for CZTSe and 2.5 μm for CZTS. For doping concentrations of combined absorber layers, both are 10^{18} cm^{-3} to reach the best performance of the solar cell.^[77] Figure 14 depicts all simulation results. CZTS/ZnSe/i:ZnO/ZnO-Al is the structure proposed by Talukder et al. The absorber layer can have a thickness between 0.5 μm and 3 μm , and its acceptor concentration can range from 1×10^{14} to $1 \times 10^{19} \text{ cm}^{-3}$, respectively. The performance parameters remain constant after the thickness reaches 2 μm while the optimized value of acceptor concentration is $1 \times 10^{18} \text{ cm}^{-3}$. The ZnSe buffer layer's thickness varies from 0.03 to 0.07 μm , and the optimizing value is 0.05 μm . Back-contact electrodes are also investigated. The role of the back electrode involves gathering the produced electron-hole pairs, while the back contact serves as a corrosion-resistant, low-recombination pathway for minority carriers, ensuring an ohmic connection.^[78] The performance of a

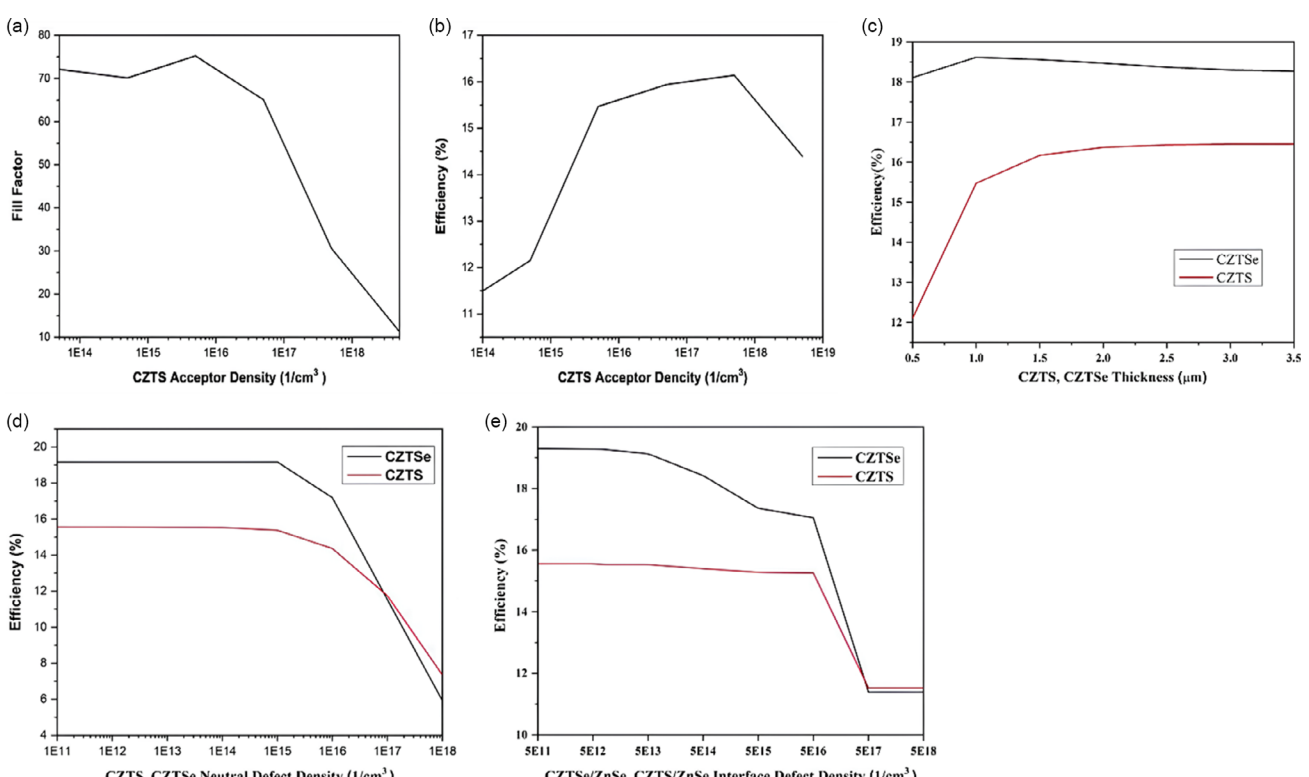


Figure 14. Simulation output results of Mo/CZTS/ZnSe/ZnO/ZnO:Al and Mo/CZTS/CZTSe/ZnSe/ZnO/ZnO:Al: a) FF and b) efficiency versus CZTS acceptor density; c) efficiency versus CZTS, CZTSe thickness d) versus CZTS, CZTSe defect density, and e) versus CZTSe/ZnSe, CZTS/ZnSe interface defect density. Reproduced with permission.^[77] Copyright 2021, Elsevier.

photovoltaic device greatly depends on the work function of the back contact, which plays a crucial role in achieving a high-quality built-in voltage (V_{bi}). Employing a back electrode with an increased work function aids in enhancing the alignment of the back energy band.^[79] In addition, the back contact is also chosen to be selenium (Se) since Se has a high work function.^[80]

7.3. Performance of CZTS Solar Cell with ZnSe Buffer Layer

All performance parameters are illustrated in **Table 10**. In the structure without CZTSe layer proposed by Srivastava, the performance parameters are efficiency $\eta = 16.24\%$, $V_{OC} = 0.825\text{ V}$, $J_{SC} = 26.53\text{ mA cm}^{-2}$, and FF = 74.14% for CZTS absorber layer with ZnO buffer layer while $\eta = 21.17\%$, $V_{OC} = 1.14\text{ V}$, $J_{SC} = 22.26\text{ mA cm}^{-2}$, and FF = 83.28% for combined absorber layer.^[77] In the work of Srivastava, the performance of the one with BSF is dramatically enhanced and provides a new idea and method for further study. The CZTSe layer could be added to other CZTS solar cells with different buffer layers to improve performance. The structure with Se back contact performs best when the absorber and buffer layer thickness are 2 and 0.05 μm . The obtained results are $\eta = 25.30\%$, $V_{OC} = 1.107\text{ V}$, $J_{SC} = 25.84\text{ mA cm}^{-2}$, and FF = 88.47%.^[80] CZTS solar cells containing ZnSe are a relatively new concept, which means that research on such a field is still in its infancy. Thus, there is ample potential space for improvement in the future.

Out of the three different structures, the one with a CZTSe layer, and the one with a Se back contact layer, exhibit efficiencies of over 20%. The proposed structure with a Se layer displays the highest efficiency, as the metal work function of Se is much higher than that of Mo. Furthermore, a higher back contact work function leads to a better outcome. Therefore, the structure Se/CZTS/CZTSe/ZnSe/ZnO/ZnO:Al could attain an even higher efficiency than 25.3%. Enhancements of this type of CZTS solar cell are still possible in the future.

8. Metal Sulfide Buffer Layer of CZTS Solar Cell

8.1. Characteristics of Metal Sulfide

Zirconium disulfide (ZrS_2) is a layered compound that belongs to group IV of the transition metal dichalcogenides (TMDCs) family. MX_2 is the general formula of dichalcogenides, where M stands for the metal component, and X denotes the chalcogenide. In this case, the specific M corresponds to Zr, and X can be either Se or S. As the quasi-two-dimensional (2D) characteristic of ZrS_2 , they have exciting optical and electronic characteristics.^[81] The compound comprises layers or sandwiches formed by chalcogens (X) on both sides, with a sheet of metal atoms (M) positioned in-between.^[82] The structure is illustrated in **Figure 15**.

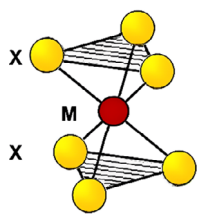


Figure 15. Crystal structure of ZrS_2 . Reproduced with permission.^[82] Copyright 2013, Elsevier.

The bonding exhibits a robust mixed covalent-ionic character within the layers, contingent upon the elements' electronegativity. However, the neighboring layers experience loose coupling through relatively weak Van der Waals (VdW) forces. Meanwhile, the material is also considered a low lattice mismatch semiconductor with a high absorption coefficient. The bandgap of ZrS_2 is between 1.2 and 2.2 eV.^[83]

As a member of the TMDC family, tungsten disulfide (WS_2) has good chemical and physical performance, which has caught tremendous attention in the research area. This material is recognized as a 2D layered-type substance comprising a metal atom sheet sandwiched between two chalcogen layers. Each W atom is surrounded by six sulfur atoms inside the sandwich layer, creating a trigonal prism configuration. The top view of the WS_2 structure is displayed in **Figure 16**. Much like graphene sheets, these sandwich layers have the ability to be mapped onto the surface of a cylinder, resulting in the formation of a triple wall (S–W–S) tube. Because of the VdW force between adjacent sheets, WS_2 shows a low lattice mismatch with the absorber layer.^[84] Moreover, the bandgap of WS_2 is from 1.5 to 2.2 eV, which matches well within the range of photovoltaic materials.^[85]

Stannic sulfide (SnS_2) has been proven to be an alternative buffer layer material.^[86] **Figure 17** schematically shows a fragment of a three-layer sandwich structure (S–Sn–S). The unit cell of this structure takes the form of a hexagonal prism featuring a Sn atom at its center. Each sulfur atom is shared among three-unit cells. All the atoms within the structure align along three-fold axes of symmetry, perpendicular to the layer's plane, passing through the lateral edges and center of the hexagonal prism, and are customarily labeled as A, B, and C.^[87] The sandwich structure represents the plane monomolecular layer with saturated valence bonds, acting as the smallest structural unit of the SnS_2 crystal in the direction perpendicular to the layers. Like WS_2 and ZrS_2 , the force between each layer in the SnS_2 crystal is VdW, and the sulfur in the boundary layers determines the packing density. SnS_2 is a cost-effective material-recommended buffer layer with a bandgap ranging from 1.82 to 2.88 eV and exhibits favorable charge mobility.^[88] Details of the comparison among three metal sulfide materials are illustrated in **Table 11**.

Table 10. Performance of proposed structures.

Reference	Proposed structure	Buffer layer	Absorber layer	Efficiency [%]	V_{OC} [V]	FF [%]	J_{SC} [mA cm^{-2}]
[77]	Mo/CZTS/ZnSe/ZnO/ZnO:Al	ZnSe (0.06 μm)	CZTS (1.0 μm)	16.24	0.825	74.14	26.53
[77]	Mo/CZTS/CZTSe/ZnSe/ZnO/ZnO:Al	ZnSe (0.06 μm)	CZTS (1.0 μm)	21.17	1.140	83.28	22.26
[80]	Se/CZTS/ZnSe/i-ZnO/ZnO:Al	ZnSe (0.05 μm)	CZTS (2.0 μm)	25.30	1.107	88.47	25.84

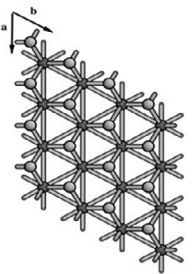


Figure 16. A top view of the WS_2 structure. Reproduced with permission.^[98] Copyright 2000, Elsevier.

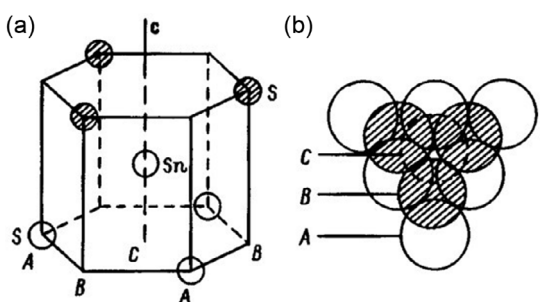


Figure 17. a) Crystal structure of SnS_2 unit cell and b) top view. Reproduced with permission.^[87] Copyright 1969, American Institute of Physics.

Table 11. Parameters of ZrS_2 in SCAPS-1D.

Parameter/Layer	ZrS_2	WS_2	SnS_2
Thickness [μm]	0.1–0.3	0.1	0.05
Bandgap [eV]	1.2–1.7	2.15	1.85
Electron affinity [eV]	4.7	4.7	4.26
Dielectric permittivity	16.4	5.1	17.7
CB effective DOS [cm^{-3}]	2.2×10^{18}	9.7×10^{18}	7.32×10^{18}
VB effective DOS [cm^{-3}]	1.8×10^{19}	1.34×10^{19}	1×10^{19}
Electron thermal velocity [cm s^{-1}]	1×10^7	1×10^7	1×10^7
Hole thermal velocity [cm s^{-1}]	1×10^7	1×10^7	1×10^7
Electron mobility [$\text{cm}^2 \text{V}^{-1} \text{s}^{-1}$]	2,300	100	50
Hole mobility [$\text{cm}^2 \text{V}^{-1} \text{s}^{-1}$]	1,300	25	25
Shallow uniform donor density N_D [cm^3]	10^{15} – 10^{18}	1×10^{18}	9.8×10^{18}
Shallow uniform acceptor density N_A [cm^3]	0	1×10^{15}	0
Defect density N_t [cm^3]	1×10^{15}	1×10^{15}	1×10^{14}
References	[83]	[85]	[58]

8.2. Improvement in CZTS Solar Cell with Metal Sulfide Buffer Layer

Moustafa et al. proposed a Mo/CZTS/ $\text{ZrS}_2/\text{ZnO}/\text{AZO}$ structure, where AZO is aluminum-doped zinc oxide material serving as a window layer. AZO possesses transparency to visible light and showcases alluring optical, acoustic, and electrical attributes.

As a result, it presents numerous possibilities for diverse optoelectronic applications. Changing the thickness of the AZO layer from 0.1 to 0.24 μm and the result shows that the thicker the window layer is, the smaller J_{sc} will be (from 26.03 to 25.94 mA cm^{-2}). As the layer thickness increases, the distance that photogenerated electrons need to travel to reach the active region also grows. Consequently, a substantial number of these carriers are lost due to recombination. Meanwhile, conversion efficiency decreases from 14.58% to 14.49% since thicker AZO would reduce the depletion width. Adjusting the absorber layer CZTS from 0.5 to 2 μm under the doping level of 10^{19} cm^{-3} , observation reveals that as the absorber layer's thickness increases, both J_{sc} and efficiency show noticeable enhancements. As the absorber layer thickness increases, more photogenerated carriers are gathered before recombination occurs. This, in turn, directly enhances the cell's efficiency.^[83] The thickness of the ZrS_2 buffer layer is varied from 0.05 to 0.3 μm while the charge carrier concentration is changed from 10^{12} to 10^{18} cm^{-3} . With the increasing carrier concentration, the efficiency is developed to 17.23% with a thickness of 0.3 μm for ZrS_2 . The main reason is that as the carrier density of the buffer layer rises, more atoms become ionized, resulting in a more significant generation of photogenerated electrons^[70]—Table 12 displays related simulation results.

For the WS_2 buffer layer, Moustafa et al. developed a Mo/CZTS/ WS_2/ZnO structure. To find the suitable thickness value of absorber CZTS layer, the setting parameter varies from 100 to 1,000 nm. As the absorber layer thickness increases, J_{sc} experiences a boost, and the efficiency follows a similar pattern. The rise in efficiency with an increase in absorber layer thickness can be attributed to the back contact recombination current density, which depends on the absorber thickness. The back contact is close to the depletion region in a thin absorber layer. Consequently, some incoming photons are absorbed near the back contact, especially those with lower energy. As a result, partial recombination of the photogenerated carriers at the back contact leads to lower efficiency.^[85] Therefore, the optimized thickness of the absorber layer is 1,000 nm. Then, a control variate method is used to study the impact of CZTS absorber layer defect density. The defect density of the absorber layer is set from 1×10^{13} to $1 \times 10^{19} \text{ cm}^{-3}$ and keeps constant of the other layer at the same time. With the rise in defect levels, recombination centers also increase, leading to a more pronounced loss in current density. This reduction in current density degrades the conversion efficiency since light-generated carriers may recombine within the energy traps.^[85] Thus, the suitable defect density should be $1 \times 10^{13} \text{ cm}^{-3}$. The bandgap energy and defect density of the WS_2 buffer layer are investigated. Through simulation, the buffer layer bandgap varies from 1.1 to 2.4 eV. After analyzing, the optimizing bandgap is chosen to be 2.2 eV. The defect density is varied from 10^{12} to 10^{21} cm^{-3} . Power conversion efficiency (PCE) increases until the density reaches 10^{18} cm^{-3} and decreases with the increased defect density of the buffer layer from 10^{18} to 10^{21} cm^{-3} . The degraded performance observed in the solar cell can be attributed to recombination with localized energy levels resulting from defects. Increasing defect density and reducing the conversion efficiency can be explained through this mechanism.^[88] Since the efficiency is almost constant

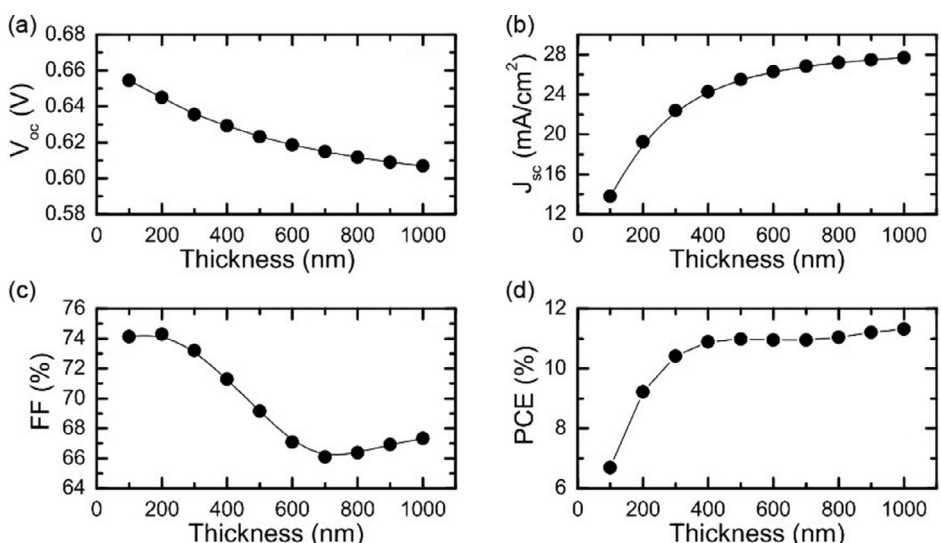
Table 12. Simulation results for ZrS₂. Reproduced with permission.^[83] Copyright 2022, Elsevier.

Obtained cell photovoltaic parameters collected at different window layer thicknesses AZO, at doping level of 10 ²⁰ cm ⁻³ .					
Thickness of window AZO [μm]	0.10	0.14	0.18	0.22	0.24
PCE [%]	14.58	14.56	14.54	14.52	14.49
J_{sc} [mA cm ⁻²]	26.03	26.00	25.97	25.93	25.94
V_{oc} [V]	0.727	0.727	0.727	0.727	0.727
FF [%]	76.97	76.97	76.97	76.97	76.97
Cell photovoltaic parameters at the various CZTS absorber layer thicknesses, at doping level of 10 ¹⁹ cm ⁻³ .					
Thickness of absorber CZTS [μm]	0.5	1.0	1.5	1.75	2.0
PCE [%]	12.89	12.92	13.91	14.15	14.40
J_{sc} [mA cm ⁻²]	25.02	25.28	25.74	25.75	26.22
V_{oc} [V]	0.593	0.661	0.717	0.709	0.708
FF [%]	80.95	80.67	79.78	77.97	78.24
Obtained cell photovoltaic parameters collected at various ZrS ₂ buffer layer thicknesses, at doping level of 10 ¹⁸ cm ⁻³ .					
Thickness of ZrS ₂ buffer layer [μm]	0.05	0.1	0.2	0.25	0.3
PCE [%]	15.95	16.39	17.15	17.24	17.6
J_{sc} [mA cm ⁻²]	23.86	25.87	26.45	26.83	27.27
V_{oc} [V]	0.772	0.773	0.774	0.775	0.776
FF [%]	82.73	82.74	83.56	82.69	81.45

between 10¹⁴ and 10¹⁸ cm⁻³, the suitable value is 10¹⁴ cm⁻³. Interface defect also plays a vital role in the performance of the solar cell. Therefore, the defect density changes from 10¹³ to 10¹⁷ cm⁻³ during the simulation. All performance parameters decrease with the increased density. The optimizing density is finally set to be 10¹³ cm⁻³. The clear indication from this result is that defect density impacts the recombination rate of electron-hole pairs within the absorber layer, leading to a decline in solar cell performance. Work function φ_m is a physical quantity

representing material surface properties' characteristics. In this work, the work function value varies from 4.7 to 5.5 eV. As the performance remains constant after 5.5 eV, the optimizing value of the work function is chosen to be 5.5 eV. **Figure 18–20** illustrate simulation results.

The team Rachidy designs a Pt/CZTSe/CZTS/SnS₂/ZnO-Al structure and investigates the effect of the thickness of different layers. The absorber layer is varied from 0.5 to 6 μm, and all the parameters exhibit a response until they reach a specific

**Figure 18.** Performance parameters a) V_{oc} , b) J_{sc} , c) FF and d) PCE versus CZTS thickness for WS₂. Reproduced with permission.^[85] Copyright 2022, Elsevier.

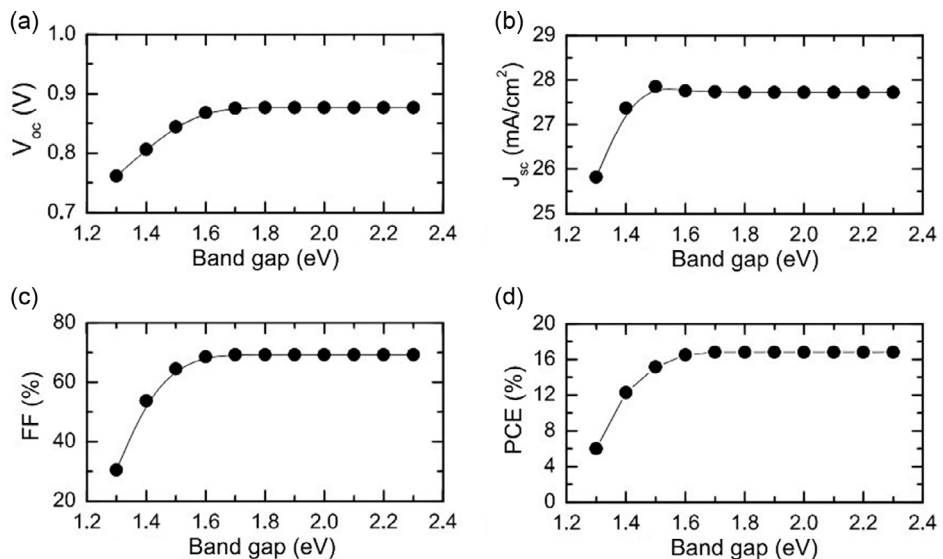


Figure 19. Performance parameters a) V_{oc} , b) J_{sc} , c) FF and d) PCE versus WS_2 bandgap for WS_2 . Reproduced with permission.^[85] Copyright 2022, Elsevier.

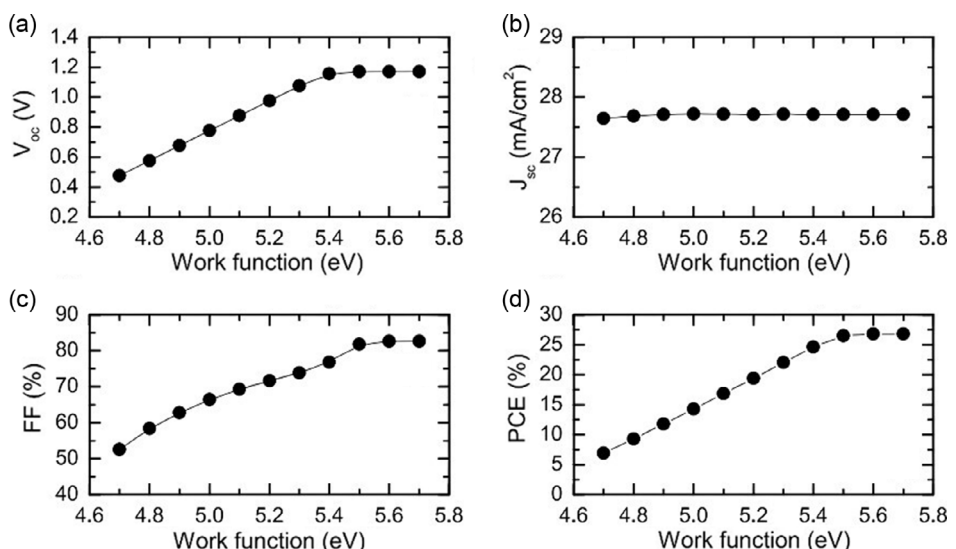


Figure 20. Performance parameters a) V_{oc} , b) J_{sc} , c) FF and d) PCE versus work function of back contact layer. Reproduced with permission.^[85] Copyright 2022, Elsevier.

thickness, at which point they level off, beyond 3 μm . This can be clarified by the idea that when the layer becomes broader or thicker, it gains more ability to capture longer wavelength photons, leading to a subsequent increase in electron–hole pairs.^[58] Regarding the decrease in fill factor beyond 2 μm , it occurs due to the emergence of resistive elements that impact the FF when dealing with greater thicknesses.^[89] Since the improvement in efficiency becomes weak after 2 μm , the optimized value of CZTS is 2 μm . Keep the absorber layer's thickness constant and vary the SnS_2 layer from 0.04 to 0.2 μm . As the buffer layer thickness increases, a marginal increase is observed in all PV parameters of the solar cell. Gradually increasing the thickness

of the buffer layer results in a systematic augmentation of the atoms within the layer available for ionization. This subsequently leads to the generation of a greater number of electrons.^[70] The optimized buffer layer is 0.05 μm . In the simulation, the thickness of the BSF layer is changed from 0.04 to 0.2 μm . J_{sc} , V_{oc} , and efficiency increase with the increase of thickness since the recombination rate is lowered. However, the parameter FF drops weakly as the high carrier concentration at the back of the cell shortens the lifetime of the minority.^[90] The acceptor concentration in the absorber layer is varied from 10^{14} to 10^{17} cm^{-3} . To balance the result, the optimizing value is 10^{16} cm^{-3} .

8.3. Performance of CZTS Solar Cell with Metal Sulfide Buffer Layer

The performance of the three structures is tabulated in **Table 13**. In the work of Moustafa, with the condition $0.05\text{ }\mu\text{m}$ AZO, $0.1\text{ }\mu\text{m}$ CZTS, and $0.3\text{ }\mu\text{m}$ buffer layer, the performance parameter of the solar cell is $J_{sc} = 27.75\text{ mA cm}^{-2}$, $V_{oc} = 0.776\text{ V}$, efficiency = 17.61% and FF = 84.75%.^[83] Until now, research on CZTS with the ZrS_2 buffer layer remains scarce, and more studies should be done. The optimizing parameters for solar cells with WS_2 buffer layer are finally improved, and the efficiency becomes 26.31%, $V_{oc} = 1.17\text{ V}$, $J_{sc} = 27.7\text{ mA cm}^{-2}$, and FF = 83.66%.^[85] This work is novel as it utilizes WS_2 as a buffer layer, resulting in great success, as demonstrated by the results. It presents a new area to fabricate Cd-free and nontoxic CZTS solar cells. However, it does not investigate the impact of the thickness of the buffer and window layers in the CZTS thin film solar cell. Rachidy's work achieves the final efficiency of 32.55%, with $V_{oc} = 0.993\text{ V}$, $J_{sc} = 50.76\text{ mA cm}^{-2}$, and FF = 64.59%.^[58] Solar cell with a BSF layer has higher efficiency with lower FF, which makes them unstable but with better working performance. To some extent, the BSF layer would reduce the lifetime of solar cells, leading to increased costs.

9. Data Integration

Figure 21 demonstrates the performance of the CZTS solar cell with various buffer layers. For the solar cell with the same material as the buffer layer, the structure with the highest conversion efficiency was selected in this figure. The CZST solar cells with Pt/CZTSe/CZTS/ $\text{In}_2\text{S}_3/\text{ZnO:Al}/\text{FTO}$ and Pt/CZTSe/CZTS/ $\text{SnS}_2/\text{ZnO-Al}$ structures exhibit nearly identical high PCEs. However, the scarcity and expense of indium (In) pose a significant drawback. Therefore, SnS_2 emerges as a preferable alternative. From an efficiency enhancement perspective, Pt/CZTSe/CZTS/ $\text{SnS}_2/\text{ZnO-Al}$ is the optimal choice. Nevertheless, this configuration exhibits a remarkably low Fill Factor (FF), which can considerably impact the solar cell's longevity and stability, increasing manufacturing costs. To strike a balance, the Mo/CZTS/ WS_2/ZnO structure presents a promising solution, with efficiency only approximately 6% lower than the highest achieved while maintaining a high FF conducive to sustainability. Meanwhile, through **Table 14**, which depicts all mentioned methods, the efficiency for solar cells with CdS is 18.2%, lower than 26.81%. The one with the WS_2 buffer layer is the best alternative. Considering the best method, substituting back contact layer Mo with high work function Pt and dope ions Al in the window layer could further improve the performance of Mo/CZTS/ WS_2/ZnO .

Table 13. Performance of proposed structures.

Reference	Proposed structure	Buffer layer	Absorber layer	Efficiency [%]	V_{oc} [V]	FF [%]	J_{sc} [mA cm^{-2}]
[83]	Mo/CZTS/ $\text{ZrS}_2/\text{ZnO/AZO}$	ZrS_2 ($0.3\text{ }\mu\text{m}$)	CZTS ($0.1\text{ }\mu\text{m}$)	17.61	0.776	84.75	27.75
[85]	Mo/CZTS/ WS_2/ZnO	WS_2 ($0.1\text{ }\mu\text{m}$)	CZTS ($1\text{ }\mu\text{m}$)	26.81	1.17	83.66	27.70
[58]	Pt/CZTSe/CZTS/ $\text{SnS}_2/\text{ZnO-Al}$	SnS_2 ($0.05\text{ }\mu\text{m}$)	CZTS ($2\text{ }\mu\text{m}$)	32.55	0.993	64.59	50.76

10. Current Challenges of CZTS Solar Cell

10.1. Performance of Real CZTS Solar Cell

The theoretical efficiency of CZTS solar cell predicted by the Shockley–Queisser (SQ) limit is 32.4%, however, its efficiency only achieved at 12.6% in real manufacturing industries.^[91] There are still three factors limit the improvement of performance, the purity of CZTS thin film, the defect of CZTS layer during deposition, the stability of CZTS phase. Since CZTS is a quaternary compound, it is more complex to control the stoichiometry, phase structure, and morphology. Some impure phases such as CuS and ZnS will be generated during the chemosynthesis of CZTS layer. Histrionics of solar cell will be influence by the impurities. Meanwhile, the recombination, generation and separation of holes and electrons are all related to the defect of crystal. Relatively lower the concentration of Cu_{Zn} and Zn_{Cu} could help to develop the performance of solar cell. Therefore, it is significant to control the low annealing temperature to adjusting the suitable defect of CZTS. The ratio of elements in CZTS compound also has an impact on the stability performance of solar cell. Recent literature reports that the best efficiency occurs when the ratio of $\text{Cu}/(\text{Zn} + \text{Sn})$ is in the domain of 0.8–0.9, Zn/Sn is in 1.1–1.3 and Cu/Sn is 1.6.^[92] Therefore, annealing CZTS properly is a great challenge.

10.2. Conductivity of CZTS Thin Film Solar Cell

Even though the CZTS compound thin film cell has several benefits, including similar characteristics to CIGS and a high Shockley–Queisser limit (SQL) of 32.4%, electrical loss that happens on every layer and within the interface is regarded as the main limiting factor.^[93] The electric loss will influence the conductivity of the CZTS solar cell. The electrical loss can be noticed through solar cell metrics such as the deterioration of V_{oc} , J_{sc} , and FF as well as the growth of series resistance R_s and shunt resistance R_{sh} . An electrical loss would occur on the CZTS absorber due to an electrical flaw, secondary phase, and high grain boundary density. A high-density charged defect might cause bandgap tailing and shorten the lifespan of a minority carrier.^[94]

10.3. Thickness of Window Layer

Loss and improper band alignment inside the window layer are two of the issues linked to this layer and its interaction. Materials that have a strong n-doping and a broad optical bandgap, along with high electric conductivity and good transparency, are required. Indium tin oxide, also known as ITO, or aluminum-doped zinc oxide is the material that is most commonly

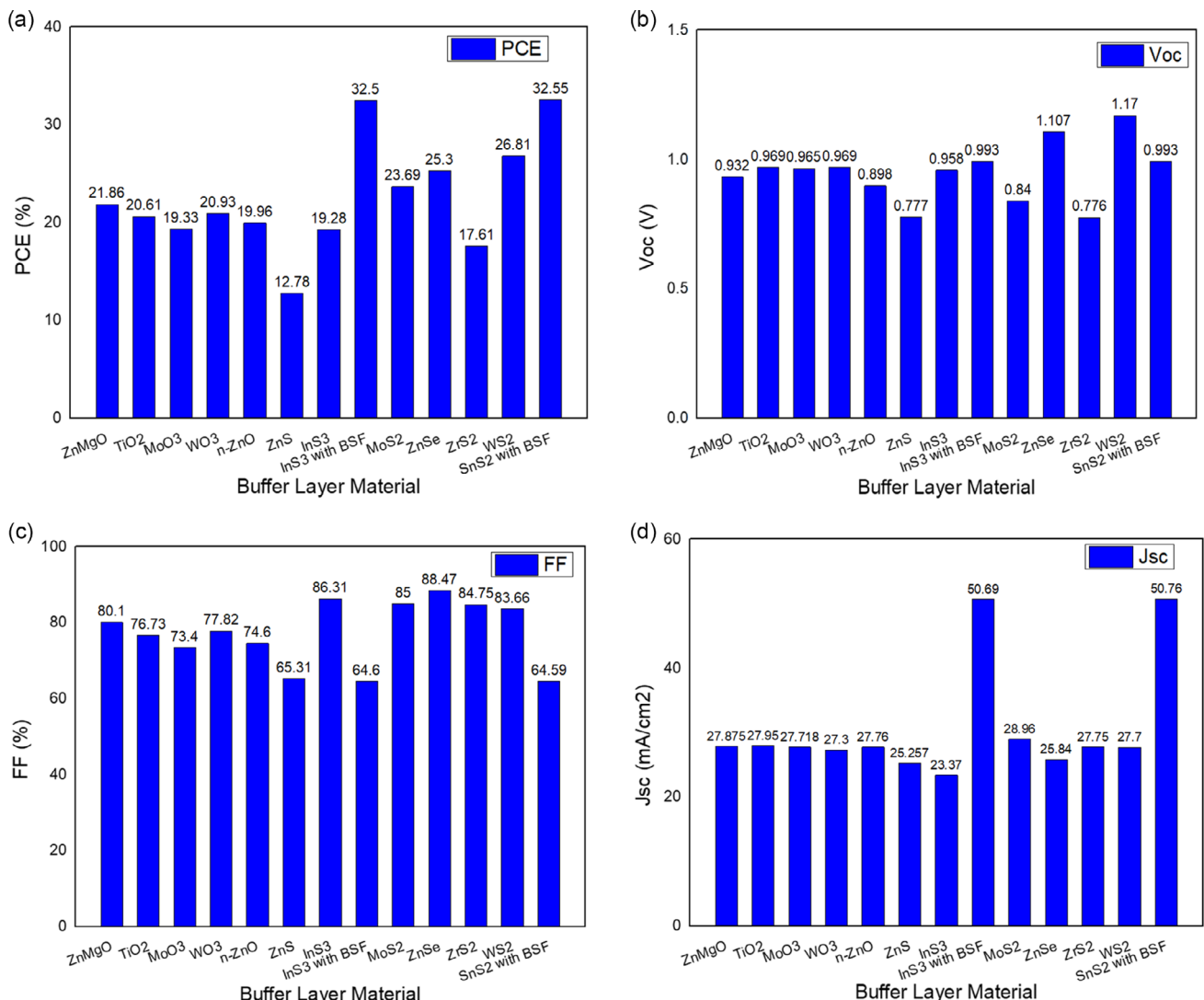


Figure 21. Performance parameters a) PCE, b) V_{oc} , c) FF and d) J_{sc} evaluation of CZTS with various buffer.

used to construct the window layer (AZO). Additionally, the window layer's thickness has a significant impact on the efficiency of solar cell. Too thick of an absorber layer will cause a drop in transmittance and a subsequent increase in optical loss, while too thin will increase transmittance at the expense of a boost in conductivity and an accompanying decrease in electric loss.^[95]

10.4. Cost and Payback Period of CZTS Solar Cell

In general, the more developed solar cell technology, the lower the fabrication cost. Much research about 1G and 2G solar cells have been done earlier. Compared to 3G solar cells, they have relatively low materialize. To reduce the cost of the 3G solar cell, learning the property of payback time is an essential parameter. The payback period means the estimated time to recover the entire investment from installing all the solar cell panels. A few factors determine it, for example, the characteristic of solar cells, which includes degeneration of performance and heat with time and the comparison of total investment and energy

production. According to different technologies, the solar cell's lifetime varies from 15 to 30 years. Compared to the last generation, thin film solar cell in 3G has smaller volume and takes less space. Therefore, lowering costs and showing comparatively favorable energy payback time is possible.^[96] Overcoming the cost challenge and understanding the payback time clearly could help to promote and commercialize the CZTS solar cell.

11. Conclusions

Compared to other types of solar cells, the CZTS solar cell offers numerous benefits, including a low cost of production and an abundance of the elements that make up the cell. In the meantime, the efficiency of solar cells made from CZTS might reach as high as 32.4%, equivalent to SQL. However, CZTS solar cells still meet some problems. The widely used CZTS with traditional buffer layer CdS harms the environment, and the production cost is high because of scarce raw materials Cd. Several studies

Table 14. Comparing various buffer layers of each mentioned method.

Reference	Structure	Buffer layer	Absorber layer/BSF	Efficiency [%]	V _{oc} [V]	J _{sc} [mA cm ⁻²]	FF [%]
[33]	Pt or Ni/CZTS/TiO ₂ /ZnO	TiO ₂ (0.1 μm)	CZTS (2.8 μm)	20.61	0.969	27.950	76.73
[33]	Pt or Ni/CZTS/MoO ₃ /ZnO	MoO ₃ (0.2 μm)	CZTS (5.2 μm)	19.33	0.965	27.718	73.40
[33]	Pt or Ni/CZTS/WO ₃ /ZnO	WO ₃ (0.02 μm)	CZTS (5.1 μm)	20.93	0.969	27.300	77.82
[35]	Mo/CZTS/ZnMgO/i-ZnO/ZnO:Al	ZnMgO (0.02 μm)	CZTS (2 μm)	21.86	0.932	27.875	80.10
[35]	Mo/MoS/CZTS/n-ZnO/i-ZnO/n-ZnO	ZnO (0.1 m)	CZTS (1.6 μm)	19.96	0.898	27.760	74.60
[46]	Mo/CZTS/ZnS/ZnO	ZnS (0.03 μm)	CZTS (2.5 μm)	12.78	0.777	25.257	65.31
[47]	Mo/CZTS/ZnS/ZnO:F	ZnS (0.002 μm)	CZTS (3.9 μm)	14.61	0.790	25.400	71.94
[52]	Mo/CZTS/In ₂ S ₃ / ZnO/ZnO:Al	In ₂ S ₃ (0.02 μm)	CZTS (2.5 μm)				
[58]	Pt/CZTSe/CZTS/ In ₂ S ₃ /ZnO:Al/FTO	In ₂ S ₃ (0.05 μm)	CZTS (2 μm) CZTSe (0.1 μm)	32.50	0.993	50.690	64.60
[56]	Mo/MoS ₂ /CZTS/In ₂ S ₃ /i-ZnO/n-ITO	In ₂ S ₃ (0.04 μm)	CZTS (3 μm)	19.03	0.795	30.060	79.63
[70]	Mo/CZTS/MoS ₂ /ZnO	MoS ₂ (0.2 μm)	CZTS (0.1 μm)	23.69	0.840	28.960	85.00
[71]	Ni/CZTS/MoS ₂ /GnP	MoS ₂ (0.04 μm)	CZTS (2 μm)	18.27	0.852	25.300	84.76
[77]	Mo/CZTS/ZnSe/ZnO/ZnO:Al	ZnSe (0.06 μm)	CZTS (1 μm)	16.24	0.825	26.530	74.14
[77]	Mo/CZTS/CZTSe/ZnSe/ZnO/ZnO:Al	ZnSe (0.06 μm)	CZTS (1 μm) CZTSe (2.5 μm)	21.17	1.140	22.260	83.28
[80]	Se/CZTS/ZnSe/i-ZnO/ZnO:Al	ZnSe (0.05 μm)	CZTS (2 μm)	25.30	1.107	25.840	88.47
[58]	Pt/CZTSe/CZTS/SnS ₂ /ZnO:Al	SnS ₂ (0.05 μm)	CZTS (2 μm) CZTSe (0.1 μm)	32.55	0.993	50.760	64.59
[83]	Mo/CZTS/ZrS ₂ /ZnO/AZO	ZrS ₂ (0.3 μm)	CZTS (0.1 μm)	17.61	0.776	27.750	84.75
[85]	Mo/CZTS/WS ₂ /ZnO	WS ₂ (0.1 μm)	CZTS (1 μm)	26.81	1.170	27.700	83.66
[100]	Mo/MoS ₂ /CZTS/CdS:Cu/ZnO	CdS:Cu (0.05 μm)	CZTS (2 μm)	18.20	1.077	26.264	64.31

on substituting toxic buffer layers with environmentally friendly materials such as metal oxide, ZnS, In₂S₃, MoS₂, and ZnSe are indicated. Meanwhile, parameters and performance are listed and compared to help browsers to do further research. In addition, the solar cell with a BSF layer of CZTSe has a better conversion efficiency, suggesting a novel strategy for optimizing the efficiency of CZTS PV cells. After integrating all statistics, the best alternative structure for substituting traditional toxic buffer layer is Pt/CZTS/WS₂/ZnO:Al. Future challenges exist. In CZTS solar cells, there is a loss of either optical or electric current, and the efficiency of such solar cells still has significant room for improvement. In the future, additional research will be needed into how CZTS solar cells may have their costs cut even further and their payback periods shortened to make it possible to commercialize third-generation solar cells.

Acknowledgements

The authors would like to acknowledge Xiamen University Malaysia for the financial support on this work. This research was funded by Xiamen University Malaysia (grant no. XMUMRF/2022-C9/IECE/0027).

Conflict of Interest

The authors declare no conflict of interest.

Author Contributions

Conceptualization, H.Z., Z.-N.N.; validation, Z.-N.N., K.-Y.C.; Writing—original draft preparation, H.Z.; Writing—review and editing, H.Z., Z.-N.N.; Supervision, Z.-N.N., K.-Y.C.; project administration, Z.-N.N.;

Funding acquisition, Z.-N.N. All authors have read and agreed to the published version of the manuscript.

Keywords

buffer layer, CZTS solar cells, nontoxic, SCAPS-1D, solar cell simulation

Received: June 12, 2023

Revised: September 6, 2023

Published online: September 27, 2023

- [1] M. Bär, I. Repins, M. Contreras, L. Weinhardt, R. Noufi, C. Heske, *Appl. Phys. Lett.* **2009**, 95, 052106.
- [2] S. Ananthakumar, R. Kumar, M. Babu, in *Emerging Nanostructured Materials for Energy and Environmental Science*, ECSW book series, Vol. 23, Springer, Cham, Switzerland **2019**, pp. 305–339.
- [3] W. Liu, H. Li, B. Qiao, S. Zhao, Z. Xu, D. Song, *Sol. Energy* **2022**, 233, 337.
- [4] Y. Zhao, C. Burda, *Energy Environ. Sci.* **2012**, 5, 5564.
- [5] M. Ravindiran, C. Praveenkumar, *Renewable Sustainable Energy Rev.* **2018**, 94, 317.
- [6] L. Guen, W. Glaunsinger, *J. Solid State Chem.* **1980**, 35, 10.
- [7] H. Matsushita, T. Ichikawa, A. Katsui, *J. Mater. Sci. Technol.* **2005**, 40, 10853.
- [8] S. Chen, X. Gong, A. Walsh, S. Wei, *Appl. Phys. Lett.* **2009**, 94, 041903.
- [9] T. Maeda, S. Nakamura, T. Wada, *MRS Online Proceedings Library (OPL)* **2009**, 1165, M04-03.
- [10] A. Walsh, S. Chen, S. Wei, X. Gong, *Adv. Energy Mater.* **2012**, 2, 400.
- [11] J. Park, Doctoral Thesis, UNSW, Sydney **2017**, <https://doi.org/10.26190/UNSWORKS/3355>.

- [12] Z. Su, G. Liang, P. Fan, J. Luo, Z. Zheng, Z. Xie, W. Wang, J. Hu, Y. Wei, C. Yan, J. Huang, X. Hao, F. Liu, *Adv. Mater.* **2020**, *32*, 2000121.
- [13] G. Liang, Z. Liu, M. Ishaq, Z. Zheng, Z. Su, H. Ma, X. Zhang, P. Fan, X. Chen, *Adv. Energy Mater.* **2023**, *13*, 2300215.
- [14] Z. Yu, C. Li, S. Chen, Z. Zheng, P. Fan, Y. Li, M. Tan, C. Yan, X. Zhang, Z. Su, G. Liang, *Adv. Energy Mater.* **2023**, *13*, 2300521.
- [15] Y. Zhao, Z. Yu, J. Hu, Z. Zheng, H. Ma, K. Sun, X. Hao, G. Liang, P. Fan, X. Zhang, Z. Su, *J. Energy Chem.* **2022**, *75*, 202208031.
- [16] P. Fan, J. Lin, J. Hu, Z. Yu, Y. Zhao, S. Chen, Z. Zheng, J. Luo, G. Liang, Z. Su, *Adv. Funct. Mater.* **2022**, *32*, 2207470.
- [17] U. Farooq, A. Shah, M. Ishaq, J. Hu, S. Ahmed, S. Chen, Z. Zheng, Z. Su, P. Fan, G. Liang, *Chem. Eng. J.* **2023**, *451*, 139109.
- [18] R. Tang, S. Chen, Z. Zheng, Z. Su, J. Luo, P. Fan, X. Zhang, J. Tang, G. Liang, *Adv. Mater.* **2022**, *34*, 2109078.
- [19] N. Ahmad, Y. Zhao, Y. Fan, J. Zhao, X. Chen, Z. Zheng, P. Fan, C. Yan, Y. Li, Z. Su, X. Zhang, G. Liang, *Adv. Sci.* **2023**, *10*, 2302869.
- [20] A. Kumar, D. Thakur, *Jpn. J. Appl. Phys.* **2018**, *57*, 8S3.
- [21] J. Marlein, K. Decock, M. Burgelman, *Thin Solid Films* **2009**, *517*, 2353.
- [22] S. Khelifi, J. Verschraegen, M. Burgelman, A. Belghachi, *Renewable Energy* **2008**, *33*, 293.
- [23] I. Lauermann, C. Loreck, A. Grimm, H. Möning, M. Lux-Steiner, C. Fischer, S. Visbeck, P. Niesen, *Thin Solid Films* **2007**, *515*, 6015.
- [24] T. Törndahl, C. Platzer-Björkman, A. Kessler, M. Edoff, *Prog. Photovolt.* **2007**, *15*, 225.
- [25] K. Lee, A. Ok, K. Park, M. Kim, Y. Baik, H. Kim, H. Jeong, *Appl. Phys. Lett.* **2014**, *105*, 083906.
- [26] N. Drissi, A. Guéddim, N. Bouarissa, *Philos. Mag.* **2020**, *100*, 1620.
- [27] H. Algarni, A. Guéddim, N. Bouarissa, I. Khan, H. Ziani, *Results Phys.* **2019**, *15*, 102694.
- [28] T. Gruber, C. Kirchner, R. Kling, F. Reuss, A. Waag, *Appl. Phys. Lett.* **2004**, *84*, 5359.
- [29] B. Maharana, R. Jha, S. Chatterjee, *Opt. Mater.* **2022**, *131*, 112734.
- [30] G. Gordon, *MRS Bull.* **2000**, *25*, 52.
- [31] T. Minami, *Semicond. Sci. Tech.* **2005**, *20*, S35.
- [32] S. Son, S. Yu, M. Choi, H. Kim, C. Choi, *Appl. Phys. Lett.* **2015**, *106*, 021601.
- [33] A. Zoubi, A. Moustafa, G. Laouini, S. Yasin, *Mater. Today* **2020**, *33*, 1769.
- [34] J. Pettersson, C. Platzer-Björkman, U. Zimmermann, M. Edoff, *Thin Solid Films* **2011**, *519*, 7476.
- [35] A. Hedibi, A. Guéddim, B. Bentria, *Trans. Electr. Electron. Mater.* **2021**, *22*, 666.
- [36] P. Sawicka-Chudy, Z. Starowicz, G. Wisz, R. Yavorskyi, Z. Zapukhlyak, M. Bester, L. Głowa, M. Sibiński, M. Cholewa, *Mater. Res. Express* **2019**, *6*, 085918.
- [37] A. Shahhoseini, B. Mozafari, *Signal Process. Renew. Energy* **2020**, *4*, 57.
- [38] K. Otoofi, M. Ranjbar, A. Kermanpur, N. Taghavinia, M. Minbashi, M. Forouzandeh, F. Ebadi, *Sol. Energy* **2020**, *208*, 697.
- [39] H. Suhail, *Int. J. Electrochem. Sci.* **2018**, *13*, 1472.
- [40] U. Saha, K. Alam, *RSC Adv.* **2018**, *8*, 4905.
- [41] S. Biswas, S. Kar, *Nanotechnology* **2008**, *19*, 045710.
- [42] X. Fang, T. Zhai, K. Gautam, L. Li, L. Wu, Y. Bando, *Prog. Mater. Sci.* **2011**, *56*, 175.
- [43] C. Yeh, Z. Lu, S. Froyen, A. Zunger, *Phys. Rev. B* **1992**, *46*, 10086.
- [44] X. Fang, T. Zhai, K. Gautam, L. Liang, L. Wu, Y. Bando, D. Golberg, *Prog. Mater. Sci.* **2011**, *56*, 201010001.
- [45] J. Hu, G. Gordon, *Sol. Cells* **1991**, *30*, 437.
- [46] E. Benzetta, A. Mahfoud, O. Elamine, *Optik* **2020**, *204*, 164155.
- [47] B. Yassine, B. Tahar, G. Fathi, *Chalcogenide Lett.* **2022**, *19*, 503.
- [48] M. Chadel, A. Chadel, M. Bouzaki, M. Aillerie, B. Benyoucef, J. Charles, *Mater. Res. Express* **2017**, *4*, 115503.
- [49] M. Chadel, M. Bouzaki, A. Chadel, M. Aillerie, B. Benyoucef, *J. Phys. Conf. Ser.* **2017**, *879*, 012006.
- [50] K. Benchouk, J. Ouerfelli, M. Saadoun, A. Siyoucef, *Phys. Procedia* **2009**, *2*, 971.
- [51] P. Pistor, R. Caballero, D. Hariskos, V. Izquierdo-Roca, R. Wächter, S. Schorr, R. Klens, *Sol. Energy Mater. Sol. Cells* **2009**, *93*, 148.
- [52] P. Lin, L. Lin, J. Yu, S. Cheng, P. Lu, Q. Zheng, *J. Appl. Sci. Eng.* **2014**, *17*, 383.
- [53] M. Sandoval-Paz, M. Sotelo-Lerma, J. Valenzuela-Jáuregui, M. Flores-Acosta, R. Ramírez-Bon, *Thin Solid Films* **2005**, *472*, 5.
- [54] P. Pistor, M. Alvarez, M. León, M. Di Michiel, S. Schorr, I. Lauermann, *Acta Crystallogr. A* **2016**, *72*, 410.
- [55] C. Khavar, R. Mahjoub, S. Samghabadi, N. Taghavinia, *Mater. Chem. Phys.* **2017**, *186*, 446.
- [56] S. Tripathi, B. Kumar, K. Dwivedi, *Optik* **2021**, *227*, 166087.
- [57] J. Fossum, R. Nasby, C. Pao, *IEEE Trans. Electron Devices* **1980**, *27*, 19937.
- [58] C. Rachidy, B. Hartiti, S. Touhtouh, S. Moujoud, A. Faddouli, F. Belhora, M. Ertugrul, S. Fadili, M. Stitou, P. Thevenin, A. Hajjaji, *Mater. Today Proc.* **2022**, *66*, 26.
- [59] O. Von Roos, *J. Appl. Phys.* **1978**, *49*, 325262.
- [60] A. Capasso, F. Matteocci, L. Najafi, M. Prato, J. Buha, L. Cinà, V. Pellegrini, A. Di Carlo, F. Bonaccorso, *Adv. Energy Mater.* **2016**, *6*, 1600920.
- [61] Z. Wang, X. Xiong, J. Li, M. Dong, *Mater. Today Phys.* **2021**, *16*, 100290.
- [62] K. Kobayashi, J. Yamauchi, *Phys. Rev.* **1995**, *51*, 17085.
- [63] S. Ahmad, S. Mukherjee, *Graphene* **2014**, *03*, 201434008.
- [64] J. Hong, Z. Hu, M. Probert, K. Li, D. Lv, X. Yang, L. Gu, N. Mao, Q. Feng, L. Xie, J. Zhang, D. Wu, Z. Zhang, C. Jin, W. Ji, X. Zhang, J. Yuan, Z. Zhang, *Nat. Commun.* **2015**, *6*, 6293.
- [65] H. Tributsch, *Sol. Energy Mater.* **1979**, *1*, 257.
- [66] T. Ferdaous, A. Shahahmadi, P. Chelvanathan, M. Akhtaruzzaman, H. Alharbi, K. Sopian, K. Tiong, N. Amin, *Sol. Energy* **2019**, *178*, 201811055.
- [67] W. Zhao, J. Pan, Y. Fang, X. Che, D. Wang, K. Bu, F. Huang, *Chem. Eur. J.* **2018**, *24*, 15942.
- [68] M. Ambrosio, E. Plesiat, P. Decleva, P. Echenique, R. Muñoz, F. Martín, *Chem. Phys.* **2022**, *557*, 111476.
- [69] S. Sandoval, Y. Yang, R. Frindt, J. Irwin, *Phys. Rev.* **1991**, *44*, 3955.
- [70] A. Bouarissa, A. Guéddim, N. Bouarissa, H. Maghraoui-Meherezi, *Mater. Sci. Eng. B* **2021**, *263*, 114816.
- [71] S. Ghosh, S. Yasmin, J. Ferdous, B. Saha, *Micromachines* **2022**, *13*, 1249.
- [72] Y. Khatami, W. Liu, J. Kang, K. Banerjee, *Proc. SPIE* **2013**, *8824*, 88240T.
- [73] S. Yasmin, J. Ferdous, B. Saha, S. Ghosh, *Proc. 7th Int. Exchange and Innovation Conf. on Engineering & Sciences (IEICES)*, Fukuoka, Japan **2021**, pp. 90–95.
- [74] C. Liu, Y. Bai, Y. Zhao, H. Yao, B. Wang, *Energy Storage Mater.* **2020**, *33*, 470.
- [75] A. Hines, P. Guyot-Sionnest, *J. Phys. Chem. B* **1998**, *102*, 3655.
- [76] Q. Zhang, H. Li, Y. Ma, T. Zhai, *Prog. Mater. Sci.* **2016**, *83*, 472.
- [77] A. Srivastava, P. Dua, R. Lenka, S. Tripathy, *Mater. Today Proc.* **2021**, *43*, 202010986.
- [78] Mamta, R. Kumar, R. Kumari, K. K. Maurya, V. N. Singh, *Mater. Today Sustainability* **2022**, *20*, 100218.
- [79] Maurya K Mamta, N. Singh, *Sol. Energy* **2021**, *230*, 202111002.
- [80] D. Talukder, R. Pal, N. Hasan, F. Wahid, *2021 Int. Conf. on Automation, Control and Mechatronics for Industry 4.0 (ACMI)*, Rajshahi, July **2021**, <https://doi.org/10.1109/ACM153878.2021.9528287>.

- [81] M. Moustafa, A. Paulheim, M. Mohamed, C. Janowitz, R. Manzke, *Appl. Surf. Sci.* **2016**, 366, 397.
- [82] M. Moustafa, A. Ghafari, A. Paulheim, C. Janowitz, R. Manzke, *J. Electron. Spectrosc. Relat. Phenom.* **2013**, 189, 35.
- [83] M. Moustafa, T. AlZoubi, S. Yasin, *Opt. Mater.* **2022**, 124, 112001.
- [84] S. Roy, P. Bermel, *Sol. Energy Mater. Sol. Cells* **2018**, 174, 370.
- [85] M. Moustafa, B. Mourched, S. Salem, S. Yasin, *Solid State Commun.* **2023**, 359, 115007.
- [86] M. Haghghi, M. Mirbashi, N. Taghavinia, D. Kim, M. Mahdavi, A. Kordbacheh, *Sol. Energy* **2018**, 167, 165.
- [87] B. Dubrovskii, *Phys. Solid State* **1998**, 40, 1557.
- [88] A. Campbell, Y. Qu, T. Gibbon, H. Edwards, V. Dhanak, D. Tiwari, V. Barrioz, N. Beattie, G. Zoppi, *J. Appl. Phys.* **2020**, 127, 101063.
- [89] M. Patel, A. Ray, *Physica B* **2012**, 407, 4391.
- [90] D. Mora-Herrera, M. Pal, J. Santos-Cruz, *Sol. Energy* **2021**, 220, 316.
- [91] W. Shockley, J. Queisser, *J. Appl. Phys.* **1961**, 32, 510.
- [92] K. Pal, K. Singh, A. Bhaduri, B. Thapa, *Sol. Energy Mater. Sol. Cells* **2019**, 196, 138.
- [93] S. Nugroho, G. Refantero, W. Septiani, M. Iqbal, S. Marno, H. Abdullah, C. Prima, N. Nugraha, B. Yuliarto, *J. Ind. Eng. Chem.* **2022**, 105, 83.
- [94] Y. Du, S. Wang, Q. Tian, Z. Zhao, X. Chang, H. Xiao, Y. Deng, S. Chen, S. Wu, S. Liu, *Adv. Funct. Mater.* **2021**, 31, 2010325.
- [95] L. Weinhardt, C. Heske, E. Umbach, P. Niesen, S. Visbeck, F. Karg, *Appl. Phys. Lett.* **2004**, 84, 3175.
- [96] O. Von, *J. Appl. Phys.* **1978**, 49, 3503.
- [97] J. Bosson, M. Birch, P. Halliday, C. Tang, K. Kleppe, D. Hatton, *Chem. Mater.* **2017**, 29, 9829.
- [98] G. Seifert, H. Terrones, M. Terrones, G. Jungnickel, T. Frauenheim, *Solid State Commun.* **2000**, 114, 245.
- [99] M. Dey, M. Dey, S. Alam, K. Das, A. Matin, N. Amin, *2016 3rd Int. Conf. on Electrical Engineering and Information Communication Technology (iCEEICT 2016)*, Dhaka, Bangladesh, September **2016**, pp. 1274–1295.
- [100] A. Jhuma, J. Rashid, *J. Theor. Appl. Phys.* **2019**, 14, 75.



Han Zhang has successfully concluded her final semester in the bachelor of electrical and electronics engineering (honors) program with her final year project thesis: Simulation of a Cu₂ZnSnS₄ (CZTS) based Photovoltaic Device using SCAPS-1D, and is slated to graduate in 2023 from Xiamen University, Malaysia. Currently, she is pursuing master's degree in electronic information engineering at Wuhan University, China. Her research interests include semiconductors and the Internet of Things.



Kah-Yoong Chan completed his Ph.D. in electrical engineering at Jacobs University Bremen in Germany in 2008. From 2005 to 2008, he served as a research scientist and later as a post-doctoral scientist at the Institute of Photovoltaics, Research Center Juelich in Germany. Dr. Chan ascended the ranks from lecturer to senior lecturer, then associate professor, ultimately attaining the position of full professor at the Faculty of Engineering at Multimedia University in 2022. His research focuses on micro- and nanofabrications, thin film materials, Internet of Things, renewable energy, metallization technologies, microelectronic reliability, and failure analysis.



Zi-Neng Ng earned his Ph.D. in engineering from Multimedia University in 2019. Prior to this, he attained a bachelor of engineering (honors) degree in electronics in 2011, followed by a master of engineering science in 2014. In 2019, he worked as a sessional staff member at Monash University, Malaysia for two semesters. His dedication and accomplishments led to his promotion as a scholarly teaching fellow at the same university in 2020. Presently, he holds the position of a full-time lecturer at Xiamen University Malaysia. Dr. Ng's research focuses on semiconducting thin film materials, sensors, solar cells, and electrochromic devices.